Spectral Nudging Impacts on Precipitation Downscaling in the Conformal Cubic Atmospheric Model, version CCAM-2504: Insights from Summer 2011

Son C. H. Truong[1], Marcus J. Thatcher[1], Phuong Loan Nguyen[2], Lisa V. Alexander[2,3] and John L. McGregor[1]

[1] The Commonwealth Scientific and Industrial Research Organisation, Victoria, Australia
[2] Climate Change Research Centre, UNSW Sydney, NSW, Australia
[3] ARC Centre of Excellence for the Weather of the 21st Century, UNSW Sydney, NSW, Australia

Correspondence to: Son C. H. Truong (sonny.truong@csiro.au)

Abstract. This study evaluates the impacts of spectral nudging on rainfall when dynamically downscaling with the Conformal Cubic Atmospheric Model (CCAM). The study focuses on the extreme 2010 – 11 La Niña, in conjunction with the Madden – Julian Oscillation (MJO), across the CORDEX – Australasia domain at 12.5 km with CCAM nested in ERA-5 reanalysis. Sixteen simulations were performed, systematically varying nudging wavelength, vertical extent, frequency, and variable choice, and evaluated against GPM-IMERG precipitation and ERA5 reanalysis. Configurations at short nudging wavelengths (~500 – 1500 km), with high-frequency updates (1h), and including pressure, wind and temperature delivered the most robust performance. These setups reduced large-scale rainfall biases, improved spatial and temporal correlations, reproduced vertical structure and moisture convergence more realistically, and achieved the closest agreement with observed mean and extreme observed rainfall. In contrast, coarse-scale (3000 km), full-column constraints, or nudging limited to pressure or wind variables degraded performance, producing oversmoothed variability, misplaced convection, and unrealistic rainfall patterns. Overall, the results demonstrate that carefully tuned spectral nudging in CCAM ~~enhances the fidelity of both mean and extreme rainfall in CCAM, while preserving~~ preserves large-scale teleconnections associated with La Niña, MJO, and ~~retaining~~ retains mesoscale variability while enhances the fidelity of both mean and extreme rainfall in this extreme 2010 – 11 La Niña event. This study strengthens confidence in CCAM downscaling for CORDEX – Australasia, with implications extending to other CORDEX domains and applications.

1 Introduction

The accurate assessment of regional climate variability and extremes is essential for supporting climate change adaptation and risk management efforts (IPCC, 2021). While general circulation models (GCMs) provide valuable insights into large-scale climate dynamics, their coarse resolution and simplified representation of regional processes limit their ability to capture local climate features, particularly extremes such as heavy rainfall events (Giorgi and Mearns, 1999; Nguyen et al., 2024). To overcome this limitation, regional climate models (RCMs) offer higher spatial resolution and a more detailed representation of topography and regional processes (Giorgi, 2019). Numerous studies have evaluated RCM performance over Australasia, demonstrating skill in reproducing regional climate features (Chapman et al., ~~2024~~2023; Howard et al., 2024; Schroeter et al., 2024; ~~Sugata~~ Narsey et al., 2025).

A central challenge for RCMs is ensuring that RCMs efficiently assimilate~~s~~ the relevant large-scale atmospheric circulation from the coarse-resolution model (e.g., forcing from the reanalysis or host GCMs) to the RCMs (von Storch et al., 2000; Feser et al., 2012). Without constraints, model biases can grow within the regional domain, resulting in considerable discrepancies from the large-scale circulations (Miguez-Macho et al., 2004). To address this, ~~a scale-selective technique (e.g.,~~ spectral nudging~~)~~ was introduced to constrain the state of the regional atmosphere at large length scales in spectral space (Von Storch et al., 2000; Kanamaru and Kanamitsu 2007; Thatcher and McGregor, 2008; Huang et al., 2021). This approach allows RCMs to develop small-scale features superimposed on the large-scale atmospheric conditions from the reanalysis or GCMs. Studies have shown that spectral nudging improves mean and extreme precipitation (Wang and Kotamarthi, 2013; Omrani et al., 2015), tropical cyclone statistics (Choi and Lee, 2015; Jin et al., 2016) and low-level wind circulation (Tang et al., 2017). Spectral nudging has also been shown to outperform other techniques, such as grid nudging, particularly in simulating extreme rainfall and low-level circulation (Liu et al., 2012; Yang et al., 2019).

The effectiveness of spectral nudging depends critically on configuration choices such as wavelengths, update frequency, vertical level, and the variables being constrained (Alexandru et al., 2009; Omrani et al., 2015, Mai et al., 2020). These parameters regulate the interplay between large-scale constraint from the reanalysis or GCMs and internal RCMs adjustment that can pose a substantial impact of the simulated circulation and precipitation. Gómez and Miguez-Macho (2017) demonstrated that nudging with wavelengths around 1000 km yields optimal results as shorter wavelengths tend to suppress fine-scale variability whereas larger wavelengths may distort synoptic conditions (Spero et al., 2018). The update frequency influences the tracks and intensification of tropical cyclone (Feser and Barcikowska., 2012; Cha et al., 2011). Moisture nudging is a debated technique. Some research cautions against it due to thermodynamic inconsistencies where temperature, moisture, and dynamical fields are no longer physically aligned when the RCM is nudged toward the ~~host GCM~~reanalysis such as ERA5 (Heikkila et al., 2010; Otte et al., 2012; Menut et al., 2024; Lai and Gan, 2025), while other studies suggest it can enhance precipitation simulation (Spero et al., 2014). In addition, biases in ERA5 moisture fields (Virman et al., 2021; Truong et al., 2022), particularly in regions with sparse observations, can introduce additional uncertainties, potentially limiting the effectiveness of moisture nudging in improving precipitation simulations. ~~The selection of vertical level at which RCMs are being nudged, or nudging profile, is primarily empirical, as different formulations can lead to various outcomes (von Storch et al., 2000; Miguez-Macho et al., 2005; Hong and Chang, 2012; Tang et al., 2017).~~ The selection of the vertical level for nudging, or the nudging profile, is largely empirical, as different choices can yield varying outcomes depending on the formulation (von Storch et al., 2000; Miguez-Macho et al., 2005; Hong and Chang, 2012; Tang et al., 2017). However, most of these investigations and their findings have been derived from limited-area RCMs such as Weather Research and Forecasting (WRF) and the Canadian RCM, where spectral nudging, typically based on fast Fourier transform (FFT), operates within a domain constrained by lateral boundary forcing. Furthermore, the conclusions drawn from these limited-area RCM studies vary depending on the model, study region, horizontal resolution, physical parameterisations, and spectral nudging configurations (Menut et al., 2024). In contrast, only a limited number of studies have explored spectral nudging in variable resolution and unstructured-grid global models, such as the Model for Prediction Across Scales (MPAS), the Conformal Cubic Atmospheric Model (CCAM). Thatcher and McGregor, (2008) developed a scale-selective filter for the variable resolution (e.g., cube-based geometry) in CCAM that differs from conventional spectral downscaling approaches by employing convolution rather than spherical harmonic FFTs (their Equation 11). They further demonstrated that a two-dimensional scale-selective filter can be efficiently approximated by a sequence of one-dimensional filters, reducing the computational cost from O(N^4) to O(N^3). Bullock et al. (2018) implemented analysis nudging, or four-dimensional data assimilation (FDDA), in MPAS-A on a 92–25 km variable-resolution mesh for January and July 2013 and highlighted the challenges associated with achieving spectral approximation on unstructured grids. Owing to their variable resolution and unstructured-grid geometries, the implementation of scale-selective nudging in variable resolution global models is inherently more complex than in conventional limited-area RCMs employing regular structured grids. These methodological differences may alter the balance between large-scale constraints and internally generated regional variability, implying that conclusions derived from traditional limited-area frameworks may not directly translate to variable resolution global models such as MPAS and CCAM. Nevertheless, systematic evaluations of nudging sensitivity in variable resolution atmospheric models remain comparatively limited. While the performance of RCMs, including CCAM, has been extensively evaluated and shown to add value to regional climate modeling in CORDEX CMIP6 (Liu et al., 2024; Ma et al., 2025; Chapman et al., 2024; Gibson et al., 2025), a critical gap remains in assessing how different spectral nudging configurations affect the performance of variable resolution models.~~While RCM performance has been evaluated in Australasia (Liu et al., 2024; Ma et al., 2025; Truong and Thatcher, 2025), to the best of our knowledge, no studies have systematically examined the sensitivity of spectral nudging configurations, in contrast to more extensive investigations over East Asia (Tang et al., 2009; Yhang and Hong, 2011), Europe (Feser, 2012), and North America (Castro et al., 2005).~~

Building on these existing challenges, our study aims to evaluate ~~This study evaluates~~ the impacts of different spectral nudging configurations on rainfall when dynamically downscaling with the Conformal Cubic Atmospheric Model (CCAM) during the extreme 2010 – 11 La Niña, in conjunction with the Madden–Julian Oscillation (MJO) and the Australian monsoon (Cai and van Rensch, 2012; Evans and Boyer-Souchet, 2012; Lisonbee and Ribbe 2021), across the CORDEX – Australasia domain. This 2010 – 11 La Niña season serves as a stringent test of CCAM's performance, as it was among the strongest La Niña events in Australia's meteorological record, rivalling historical extremes (BoM, 2012) led to widespread flooding in many regions over Australia including Queensland, Victoria, New South Wales, and Western Australia (Ummenhofer et al. 2015). The season was also marked by increased tropical cyclone activity, notably severe tropical cyclone Carlos over Darwin (367.6 mm/day) and Yasi over Queensland (471 mm/day) (BoM, 2012). At the national level, the cost of recovery from natural disasters across Australia in 2010 and early 2011 was estimated to surpass AU$12 billion in government expenditure (Table 25.1, Karoly and Boulter, 2013). In this study, we aim to:

1. Evaluate the ability of CCAM to reproduce ~~regional rainfall and~~ large-scale circulation during the extreme 2010 – 11 La Niña;
2. Quantify the influence of nudging parameter choices on the representation of mean and extreme rainfall; and
3. Identify parameter combinations that improve the fidelity of regional rainfall simulations over Australasia during the extreme event.

The paper is organized as follows: Section 2 outlines the data and methods; Section 3 describes study results; and Section 4 discusses the findings and conclusions.

2 Data and methods

2.1 ERA5 reanalysis

The ERA5 reanalysis, produced by the European Center for Medium-Range Weather Forecasts (ECMWF), is based on the global Numerical Weather Prediction (NWP) model Integrated Forecast System (IFS) version CY41R2 (Hersbach et al., 2020). The model provides hourly estimates of atmospheric variables, at a horizontal resolution of 31 km and 137 vertical levels from the surface to 0.01 hPa. The data is available on both surface (e.g., total precipitation) and 37 pressure levels (e.g., vertical winds). The variables used in this study are wind speed, temperature, specific humidity, and mean sea level pressure. In this study, ERA5 is preferred over higher-resolution datasets such as Atmospheric Regional Reanalysis for Australia version 2 (BARRA2) (Su et al., 2025) due to its global coverage, which is better suited for CCAM.

2.2 Observations

In this study, we evaluate simulated precipitation using the Integrated Multi-satellite Retrievals for the Global Precipitation Measurement (GPM) IMERG Final Run product (Version 07; Huffman et al., 2019), distributed by NASA Goddard Earth Sciences Data and Information Services Center (GES DISC)~~GES DISC~~. The level-3 IMERG fields provide 0.1° x 0.1° coverage from 60°S-60°N and merge estimates from a constellation of passive-microwave and infrared sensors, intercalibrated to monthly rain-gauge analyses; we use the daily accumulation (mm day^{-1}). To benchmark observational uncertainty, particularly pronounced over the equatorial and data sparse regions (Alexander et al. 2025; Nguyen et al., 2022), we include two additional daily products: the Global Precipitation Climatology Project (GPCP) daily CDR v3.2 (Huffman et al., 2023) and the Climate Prediction Center morphing method (CMORPH) v1.0 CRT (Joyce et al., 2004; Xie et al., 2017). The GPCP v3.2 provides globally complete 0.5° x 0.5° analyses from June 2000 to present, blending low-orbit satellite microwave data, geosynchronous-orbit satellite infrared data, sounder-based estimates, and surface rain gauge observations. The CMORPH v1.0 CRT provides bias-corrected, reprocessed estimates on a 0.25° grid with native 30-min resolution aggregated to daily for 1998-2023. As a high-quality continental reference over Australia, we also use AGCD v1.0.0 daily rainfall, a 0.05° x 0.05° gridded gauge-based analysis derived from quality-controlled station data across mainland Australia and Tasmania (Jones et al., 2009). These datasets are selected for their demonstrated consistency in representing daily precipitation (Imran and Eva~~á~~ns 2025) and extremes (Alexander et al., 2020; Nguyen et al., 2020).

2.3 Model description

The climate model used for the study is Conformal Cubic Atmospheric Model (CCAM) (McGregor and Dix, 2008), developed by the Commonwealth Scientific and Industrial Research Organisation (CSIRO). CCAM is an open-source global stretched-grid non-hydrostatic numerical model, which has been extensively used for regional climate studies (Gibson et al., 2024, Liu et al., 2024; ~~Sugata~~ Narsey et al., 2025). CCAM can be operated with either a stretched grid or with a global quasi-uniform grid (Truong et al., 2025; Truong and Thatcher, 2025), driven by sea-surface temperatures (SSTs) and sea ice concentrations (Hoffmann et al., 2016; Zhang et al., 2024). This makes CCAM useful for regional climate simulations where errors arising from lateral boundary conditions can be avoided, although physical parameterisations must operate successfully over a range of spatial scales. The amount of stretching is described by a Schmidt factor where 1 indicates a quasi-uniform grid and values greater than 1 imply an increasing amount of grid stretching. CCAM includes parameterisations for radiation (Freidenreich and Ramaswamy, 1999; Schwarzkopf and Ramaswamy, 1999), convection (McGregor, 2003), gravity wave drags (Chouinard et al., 1986), and boundary layer turbulent mixing (Hurley, 2007). CCAM also includes the Community Atmosphere Biosphere Land Exchange (CABLE) land-surface scheme (Kowalczyk et al., 2006), the Urban Climate and Energy Model (UCLEM) ~~urban~~ parameterisation (Thatcher and Hurley, 2011) and a cloud microphysics scheme based on Rotstayn (1997). To constrain large-scale circulation, ~~Thatcher and McGregor (2008) introduced a scale-selective filtering approach (e.g., spectral nudging), based on convolution-based scheme, for CCAM that constrains only the large length scales while allowing regional atmosphere at small length scales to evolve freely.~~ Thatcher and McGregor (2008) introduced a novel scale-selective filtering method (e.g., Gaussian filter rather than a simple cut-off) for CCAM, which differs from traditional spectral nudging that relies on Fourier-based methods. Instead of using spherical harmonic FFTs, their approach employs convolution filters on the model's native grid and a nudging wavelength can be larger than the high-resolution domain. They demonstrated that the 2D scale-selective filter could be approximated by a sequence of 1D filters, reducing computational complexity from $O(N^4)$ to $O(N^3)$, making it computationally efficient for large-scale global simulations like CCAM.

2.4 Model configuration

There are a limited number of studies exploring spectral nudging in variable resolution global models. Thatcher and McGregor (2008) applied spectral nudging to surface pressure, wind, and temperature in CCAM, finding that it reasonably reproduced downscaled predictions from National Centers for Environmental Prediction Global Forecast System (NCEP GFS) 0.58 analyses. More recently, Bullock et al. (2018) employed nudging in MPAS-A, emphasizing that further research is needed to determine the optimal nudging selection for temperature, humidity, and wind, as well as the most effective vertical levels for applying nudging. Building on the work of Thatcher and McGregor (2008) in variable resolution model (i.e., CCAM) and other related limited-area model findings (Menut et al., 2024), this study further investigates the impacts of spectral nudging on precipitation, with a total of 16 simulations conducted using CCAM. These simulations are grouped into seven categories, as summarized in Table 1. Each simulation differs based on four key nudging options: variables (pressure [p], zonal and meridional wind components [u] and [v], temperature [t], and specific humidity [q]), horizontal wavelength (in km), update frequency (in hours), and vertical level. Simulation names follow the format: *[VARs]_[Wavelength]_[Frequency]_[Level]*, where "VARs" represents the nudged variables (e.g., PUVTQ), "Frequency" is the update interval (e.g., 1h), "Level" indicates the vertical level at which the lowest model being nudged to the top of the atmosphere and "Wavelength" is the horizontal nudging wavelength (e.g., 3000 km).

To understand the impact of the spectral nudging, a definition of the filter length-scale is required. In Thatcher and McGregor (2008), the Gaussian filter is defined by Eq. 1:

$$\exp\left(-\frac{\pi^2 d^2}{\varepsilon}\right) \qquad (1)$$

Here ϵ is a constant that defines the filter length-scale and d is the distance from the centre of the Gaussian filter in radians. Typically, CCAM defines the filter length-scale as a function of the Schmidt factor, S, that controls the amount of grid stretching. This is so that the filter length-scale automatically is reduced as the grid is increasingly stretched. Using the following expression (Eq. 2) approximately makes the filter length-scale the size of the high-resolution region on the stretched CCAM grid.

$$\epsilon = \frac{\pi^4}{18 \times S^2} \qquad (2)$$

Note that CCAM will limit the maximum filter length-scale to a value that corresponds to S=3.333. There are multiple ways to define the width of the Gaussian filter length-scale. Thatcher and McGregor (2008) used the Full-Width-at-Half-Maximum (FWHM) definition. For the CCAM grid configuration used in this paper, we obtain FWHM=10.6 radians or approximately 2400 km in diameter. However, this is often unintuitive for users of the CCAM model. Hence an alternative definition that represents 99.7% of the Gaussian is used where the diameter of the Gaussian filter is $\pi/18$ radians or approximately 3000 km for S=3.333. For consistency with previous literatures, we will use the 99.7% definition for the filter length scale (e.g., 3000, 1500, and 500 km) in the rest of this paper.

~~To assess the impacts of spectral nudging on precipitation, a total of 16 simulations were conducted using CCAM arranged into seven groups (Table 1). *"Ctrl"* group includes no nudging. *"P_var"* group comprised three simulations (P_3000_1h_L0.85, P_1500_1h_L0.85, and P_0500_1h_L0.85) in which only surface pressure was spectrally nudged above the planetary boundary layer (PBL) at wavelengths of 500, 1500, and 3000 km, with a relaxation interval of 1h. In *"PUV"* group, both surface pressure and horizontal wind components were nudged at the same wavelengths and interval. *"PUVT_1h"* group extended nudging variables to include surface pressure, horizontal wind, and temperature, while *"PUVT_3h"* group used identical variables and wavelengths but a weaker nudging strength, with the relaxation interval increased to 3h. *"PUVT_L"* group tested the sensitivity to vertical level at which nudging is applied, including (i) full-~~

~~column (L1, surface to top of the atmosphere), and (ii) half column (L0.5, mid to top of the atmosphere). Finally, *"PUVTQ"* simulation nudged surface pressure, horizontal wind, temperature, and specific humidity with a wavelength of 3000 km. The simulations are initialised using ERA5 reanalysis at 00 UTC on November 1, 2010, and run for a period of 5 months at 12 km horizontal resolution and 54 vertical level. A 1-month spin-up period is used to stabilise the model. The SST evolution is driven from ERA5 reanalysis.~~The ***"Ctrl"*** group serves as the baseline simulation with "no nudging", initialized with ERA5 reanalysis data at 00 UTC on November 1, 2010, and allowed to evolve freely. This setup provides a reference for comparing the influence of nudging on model performance, with dynamics driven solely by initial conditions and internal processes. In the ***"P_var"*** group, three simulations (P_3000_1h_L0.85, P_1500_1h_L0.85, and P_0500_1h_L0.85) were conducted, where surface pressure was nudged above the PBL at wavelengths of 500 km, 1500 km, and 3000 km with a 1-hour relaxation interval. Based on Truong et al. (2025), which showed that horizontal resolution differences in variable resolution models affect tropical cyclone intensity, pressure nudging was applied first to assess its influence on large-scale circulation. The ***"PUV"*** group extended the nudging to include both surface pressure and horizontal wind components, using the same wavelengths and relaxation interval as the ***"P_var"*** group. This configuration assesses the combined impact of nudging both wind and pressure, which is crucial for influencing large-scale dynamics (e.g., MJO, monsoonal flow) and convection (e.g., TC). In the ***"PUVT_1h"*** group, additional variables, including temperature, were nudged alongside pressure and wind, using the same wavelengths and relaxation interval as in the previous groups. This simulation evaluates the impact of thermal dynamics on heat and moisture fluxes, which influence convection and precipitation. The ***"PUVT_3h"*** group replicated the ***"PUVT_1h"*** setup but with a weaker nudging strength and a 3-hour relaxation interval to assess the sensitivity of model performance to weaker nudging. Various studies have documented that nudging within the boundary layer can artificially suppress convection (Heikkilä et al., 2010; Otte et al., 2012; Spero et al., 2014), potentially affecting tropical cyclones during our study period, the extreme 2010–11 La Niña. In this study, we applied nudging at a fixed layer (e.g., 850 hPa) by default, rather than dynamically nudging to the top of the simulated boundary layer height, in order to save computational resources. We further conducted two additional sensitivity tests on pressure levels (i.e., ***"PUVT_L"***) with two setups: full-column nudging (L1), which applies nudging from the surface to the top of the atmosphere, and half-column nudging (L0.5), which limits nudging to the mid-to-upper atmosphere. Given the inconsistent results of moisture nudging in limited-area models (Menut et al., 2024, Spero et al., 2014), we conducted additional sensitivity test to assess whether moisture nudging would further improve or adversely affect our precipitation simulation (***"PUVTQ"***). ~~exp exp~~ All simulations were initialized using ERA5 reanalysis data at 00 UTC on November 1, 2010, and were run for a period of 5 months at a 12 km horizontal resolution and 54 vertical levels. A 1-month spin-up period was used to stabilize the model. The sea surface temperature (SST) evolution was driven from ERA5 reanalysis.

Table 1 Summary of the 16 simulations conducted in this study. ~~***Each simulation differs based on four key nudging options: variables (pressure [p], zonal and meridional wind components [u] and [v], temperature [t], and specific humidity [q]), horizontal wavelength (in km), update frequency (in hours), and vertical level. Simulation names follow the format: [VARs]_[Wavelength]_[Frequency]_[Level], where "VARs" represents the nudged variables (e.g., PUVTQ),***~~

~~*"Wavelength" is the horizontal nudging wavelength (e.g., 3000 km), "Frequency" is the update interval (e.g., 1h), and "Level" indicates the vertical level at which the model being nudged to the top of the atmosphere (e.g., 0.85 for 0.85 sigma level).*~~ ***The simulations are grouped by nudging configuration to facilitate comparison.***

EXP. group	EXP.	EXP. name	Nudging variables	Wavelength (km)	Update frequency	Lowest Level (hPa)
CTL	1	Ctrl	-	-	-	-
P_var	2	P_3000_1h_L0.85	p	3000	1h	850~~0.85~~
	3	P_1500_1h_L0.85		1500	1h	850~~0.85~~
	4	P_0500_1h_L0.85		500	1h	850~~0.85~~
PUV	5	PUV_3000_1h_L0.85	p, u, v	3000	1h	850~~0.85~~
	6	PUV_1500_1h_L0.85		1500	1h	850~~0.85~~
	7	PUV_0500_1h_L0.85		500	1h	850~~0.85~~
PUVT_1h	8	PUVT_3000_1h_L0.85	p, u, v, t	3000	1h	850~~0.85~~
	9	PUVT_1500_1h_L0.85		1500	1h	850~~0.85~~
	10	PUVT_0500_1h_L0.85		500	1h	850~~0.85~~
PUVT_3h	11	PUVT_3000_3h_L0.85	p, u, v, t	3000	3h	850~~0.85~~
	12	PUVT_1500_3h_L0.85		1500	3h	850~~0.85~~
	13	PUVT_0500_3h_L0.85		500	3h	850~~0.85~~
PUVT_L	14	PUVT_3000_1h_L0.5	p, u, v, t	3000	1h	~~0.5~~500
	15	PUVT_3000_1h_L1	p, u, v, t	3000	1h	~~1~~surface
PUVTQ	16	PUVTQ_3000_1h_L0.85	p, u, v, t,q	3000	1h	850~~0.85~~

We first evaluated model performance using bias maps, time-series correlation, standard deviation, root-mean-square-error (RMSE) and percentile-based metrics for extreme events, along with Taylor diagrams for spatial skill and quantile-quantile plots to assess extreme precipitation distributions. We followed Isphording et al. (2024)'s ~~introduce a set of minimum~~ standard metrics benchmarking for regional climate models in estimating four fundamental characteristics (intensity, spatial distribution, seasonal cycle and changes over time) of rainfall over Australia. Here, we adopted the mean absolute percentage error (MAPE) and the spatial correlation coefficient (Scor) as other two metrics not being relevant given the short simulation that we are performing. The MAPE is defined following Eq. (~~1~~3)

$$\mathrm{MAPE} = \frac{1}{n}\sum_{i=1}^{n}\frac{|\mathrm{model}_i - \mathrm{obs}_i|}{\mathrm{obs}_i} \qquad (\cancel{1}3)$$

~~,~~ where n is the number of grid cells in the spatial domain. Scor quantifies pattern alignment, ranging from 0 (no match) to 1 (perfect match). In addition to precipitation-based metrics, we also examined the large-scale moisture transport by calculating the divergence of water vapor flux at ~~700~~ 875 hPa. The water vapor flux divergence is defined following Eq. (~~2~~4)

$$\nabla(Vq) = \frac{\partial}{\partial x}(uq) + \frac{\partial}{\partial y}(vq) \qquad (\cancel{2}4)$$

where q denotes the specific humidity, and u and v are the zonal and meridional wind components, respectively.

To facilitate our regional analysis, the CORDEX–Australasia domain is partitioned into three subregions (R2, R4, and R5), which represent distinct climatic and synoptic regimes: R2 (northwestern Australia), R4 (northeastern Australia), and R5 (southeastern Australia) (Fig. 1). These are also regions that were most affected by strong tropical cyclones and major flooding during the extreme 2010–11 La Niña (Karoly and Boulter, 2013). We also include the Maritime Continent (MC) and the southwestern pacific as R1 and R3 to examine the mean and extreme precipitation over these convective (R1) and orographic (R3) regions; ~~albeit~~ the R1 and R3 partially belong to the CORDEX – SEA domain. Finally, R6 is defined as the entire domain. This subregional framework provides a consistent basis for examining precipitation processes across a broad spectrum of climatic drivers, including tropical–extratropical interactions, the Madden–Julian Oscillation (MJO), El Niño–Southern Oscillation (ENSO) teleconnections, and the austral-summer monsoon during the anomalously wet spring and summer of 2010 – 11.

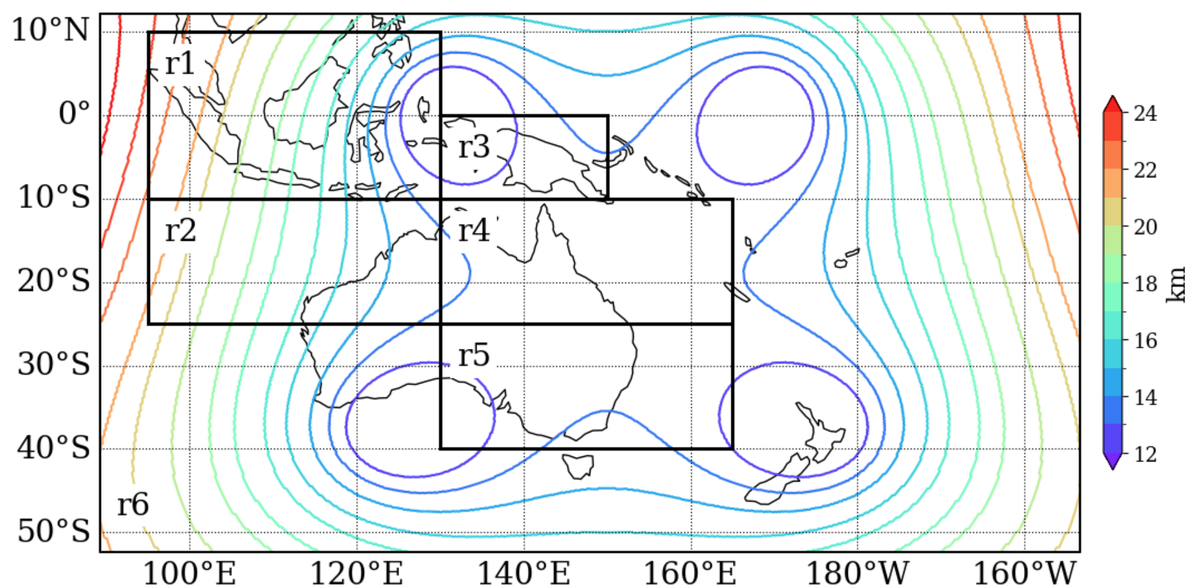

Figure 1 CCAM simulation domain with grid resolution ranging from 12 to 25 km, shown in contour colours. The study domain is divided into six subregions, labelled R1 to R6, representing the Maritime Continent, northwest Australia, southwestern pacific, northeast Australia, southeast Australia, and the whole simulated domain (50°S – 10°N, 90°E – 150°W), respectively.

3 Results

3.1 Mean precipitation

3.1.1 Spatial variability of precipitation

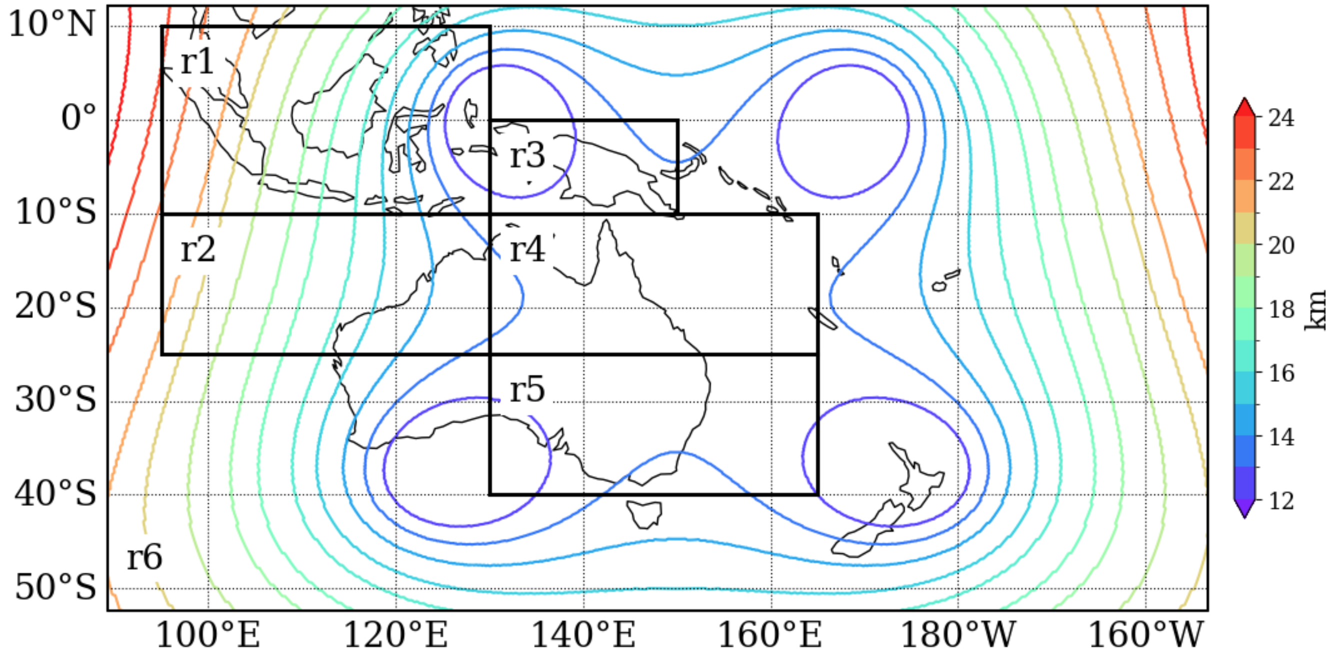

~~***Figure 1 CCAM simulation domain with grid resolution ranging from 12 to 25 km, shown in contour colours. The study domain is divided into six subregions, labelled R1 to R6, representing the Maritime Continent, northwest Australia, southwestern pacific, northeast Australia, southeast Australia, and the whole simulated domain (50°S – 10°N, 90°E – 150°W), respectively.***~~

~~To facilitate our regional analysis, the CORDEX–Australasia domain is partitioned into three subregions (R2, R4, and R5), which represent distinct climatic and synoptic regimes: R2 (northwestern Australia), R4 (northeastern Australia), and R5 (southeastern Australia) (Fig. 1). We also include the Maritime Continent (MC) and the southwestern pacific as R1 and R3 to examine the mean and extreme precipitation over these regions albeit the R1 and R3 belong to the CORDEX — SEA domain. Finally, R6 is defined as the entire domain. This subregional framework provides a consistent basis for examining precipitation processes across a broad spectrum of climatic drivers, including tropical–extratropical interactions, the Madden–Julian Oscillation (MJO), El Niño–Southern Oscillation (ENSO) teleconnections, and the austral-summer monsoon during the anomalously wet spring and summer of 2010 – 11.~~

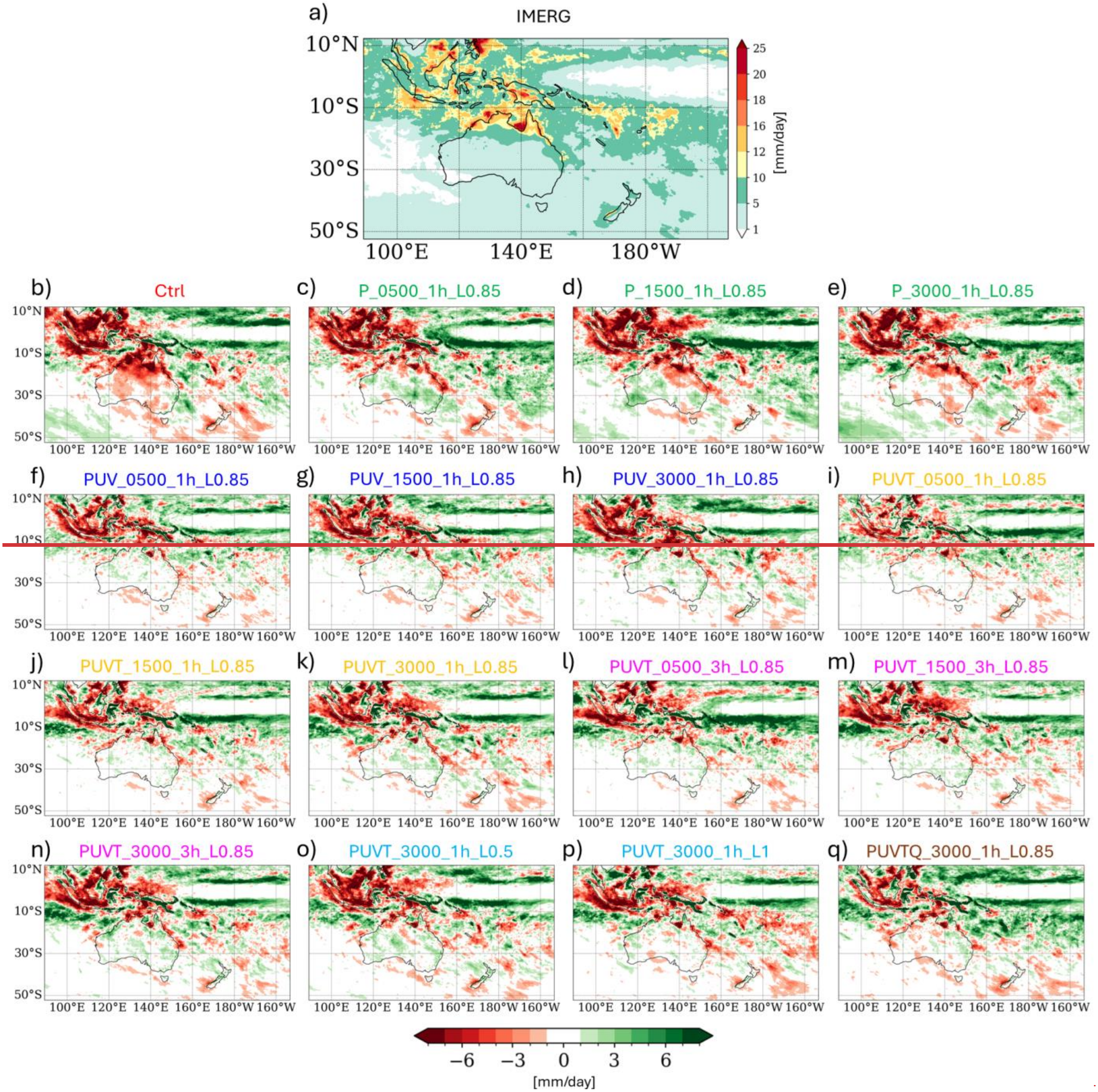

~~*Figure 2 (a) The averaged precipitation from December 2010 to March 2011 over the study domain (mm day^{-1}) for IMERG; and (b)–(q) the bias between 16 simulations described in Table 1.*~~

The averaged IMERG precipitation exceeded 25 mm day^{-1} over the MC and the western Pacific, with enhanced across northern and northeastern Australia (Fig. 2a). In contrast, central and southern Australia received less than 5 mm day^{-1}. In general, IMERG, GPCP, and CMORPH exhibit similar spatial distributions (Fig. S1) and timeseries (Fig. S2), capturing the broad rainfall patterns during the extreme 2010 – 11 La Niña. The only notable difference is that IMERG tends to have slightly more intense precipitation, particularly in the tropical region (R1) and over the Gulf of Carpentaria (R4) compared to GPCP and CMORPH.

In the CCAM simulations, the *Ctrl* displays substantial regional biases relative to IMERG (Fig. 2b). A wet bias (green shading) dominates the equatorial western Pacific, suggesting an excessive convective activity north of Papua New Guinea, while a dry bias (red shading) prevails across northern and eastern Australia, the MC, indicating a systematic underestimation of tropical convection activities. Over Australia, the *Ctrl* shows strong dry biases (>5 mm day^{-1}) in the north and similar, though less pronounced, bias in the southeast, underscoring the challenges in reproducing observed precipitation (Fig. 2b). The time series of spatially averaged daily rainfall for IMERG and AGCD over Australia shows strong agreement (r = 0.94), with similar timing and intensity of rainfall events throughout the study period (Fig. S3).~~, although IMERG is almost always wetter than AGCD, which may slightly reduce the dry bias.~~ However, the spatial distribution of correlation and RMSE between AGCD and IMERG is low across much of Australia (Fig. S3b-c). This discrepancy arises because grid-point comparisons are sensitive to small spatial and timing differences, while spatial averaging suppresses small-scale variability and highlights large-scale signals such as the MJO, monsoonal circulation, and frontal systems, which both datasets capture more consistently (Fig. S3a).

Most nudged simulations reduce these continental biases, with biases over Australia generally constrained within ±2 mm day^{-1} (Fig. 2c-q). Improvements are most pronounced in the eastern and southern subregions, where large dry biases in the *Ctrl* are substantially diminished. However, model performance remains limited in specific regions, such as the wet bias observed in the high-elevation areas of Papua New Guinea and the dry bias over the Gulf of Carpentaria. These biases coincide with significant observational uncertainties (Alexander et al., 2020), as the three precipitation products differ markedly in their representation of precipitation in region R3 and R4 (Fig. S1). These results suggest that while spectral nudging substantially improves rainfall representation over continental Australia, it is less effective in correcting tropical precipitation biases, which may be linked to convective parameterisation ~~parameterization~~ and/or the impacts of horizontal resolution.

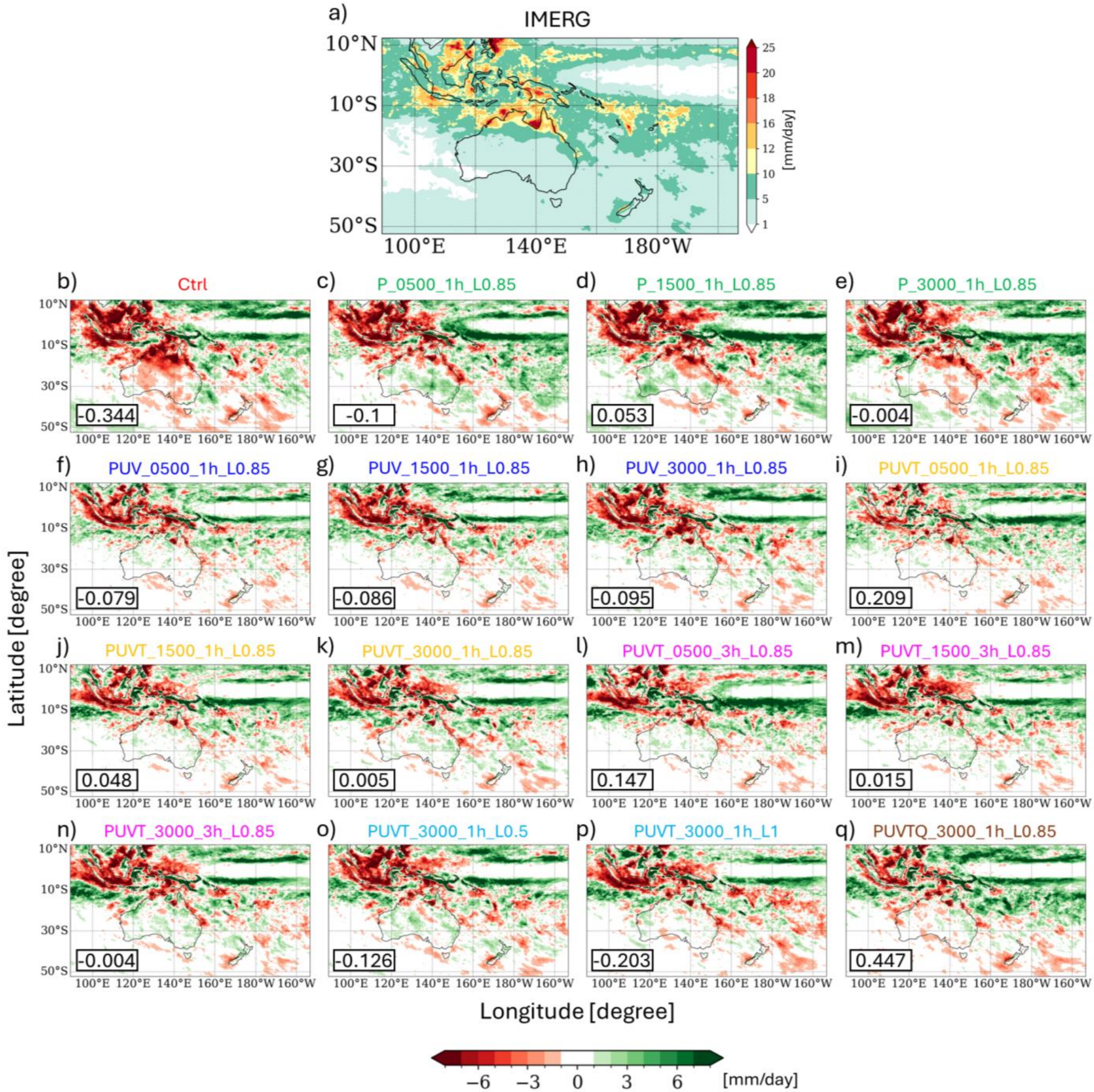

Figure 2 (a) The averaged precipitation from December 2010 to March 2011 over the study domain (mm day^{-1}) for IMERG; and (b)–(q) the bias relative to IMERG for each of the 16 simulations. Black box in the lower left indicates the domain averaged values. Different colours in the header of each panel indicate the grouped simulations in Table 1.

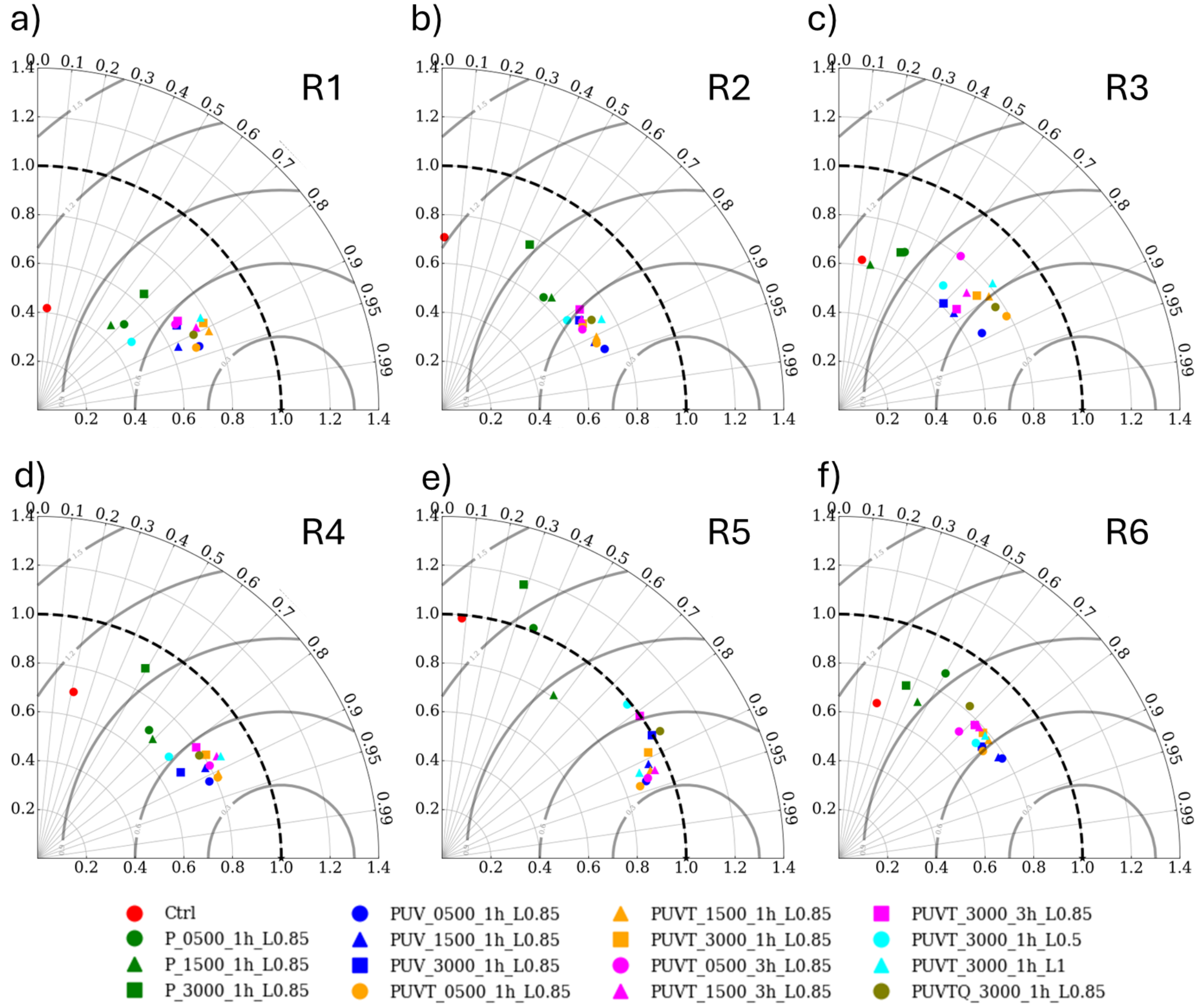

~~*Figure 3 Taylor diagrams of daily precipitation averaged from December 2010 to March 2011 for six subregions (R1–R6), comparing 16 CCAM simulations with IMERG. Radial axis (distance from origin) represents standard deviation of the simulated precipitation (normalized by the observed standard deviation, IMERG). Angular axis (angle from x-axis) represents correlation coefficient between models and IMERG. Solid gray concentric arcs represent the cantered root-mean-square error (RMSE) between model and IMERG [a distance from the reference point on x-axis at (1,0)]. Coloured markers denote simulation groups (legend).*~~

Next, we assess the model performance over the six regions presented in Fig. 1 using Taylor diagrams~~We used a Taylor diagram~~ of mean precipitation distribution ~~across six subregions~~ (Fig. 3) to quantify spatial skill in terms of correlation (R), normalized standard deviation (nSD), and root-mean-square error (RMSE). The *Ctrl* shows very low correlations (R = 0.05 – 0.25), strongly underestimated variance across all domains (nSD ~ 0.2 – 0.4), and RMSE consistently largest across all regions, underscoring its inability to reproduce the spatial-organized precipitation. In contrast, most nudged simulations achieved substantially higher skill, with R values of 0.80 – 0.95, nSD between 0.5 and 0.9, and markedly reduced RMSE (Fig. 3 and Fig. S4). Improvements were most pronounced over Australian continent (R2, R4, and R5), where several configurations reached R ≥ 0.9 and nSD close to 1, while performance was weaker in convective (R1) and orographic (R3) regions, where R remained somewhat lower (~0.75 – 0.85) and RMSE larger. It is also worth mentioning that observational uncertainties are significant in estimating both mean precipitation and extremes in R1 and R3 (Nguyen et al., 2020; Alexander et al., 2020), which could explain the "weaker performance" observed in simulations over these regions.

Examining further into each nudged simulations indicate that *P_var* groups yields modest improvements over Australia. Furthermore, correlations remain weak in convective and orographic regions (e.g., R1, R3), rarely exceeding R = 0.6 and with relatively large RMSE. *PUV* groups performs better, especially in R4 and R5 where correlations approach 0.9 and RMSE is reduced, though tropical biases persist. The *PUVT_1h* and *PUVT_3h* groups produce the most balanced results, with R consistently ≥ 0.8 – 0.9, nSD less than 1, and lowest RMSE across regions, particularly for shorter wavelength, 1-h updates (500 – 1500 km, L0.85). By contrast, simulations with adding moisture (*PUVTQ*) or vertical levels (*PUVT_L*) exhibit inconsistent performance across regions, sometimes improving correlation but often at the cost of reduced variance. Collectively, these results align with previous discussion that shorter wavelength, frequent, multi-variable nudging (*PUVT*) offers better spatial representation of precipitation, whereas vertical nudging of either from surface or mid- to the top of the atmosphere lead to regionally biased outcomes. Our analysis of the Taylor diagram comparing CCAM simulations to GPCP produced results similar to those obtained with IMERG, reinforcing our previous conclusion without altering the overall findings (Fig. ~~S4~~S5).

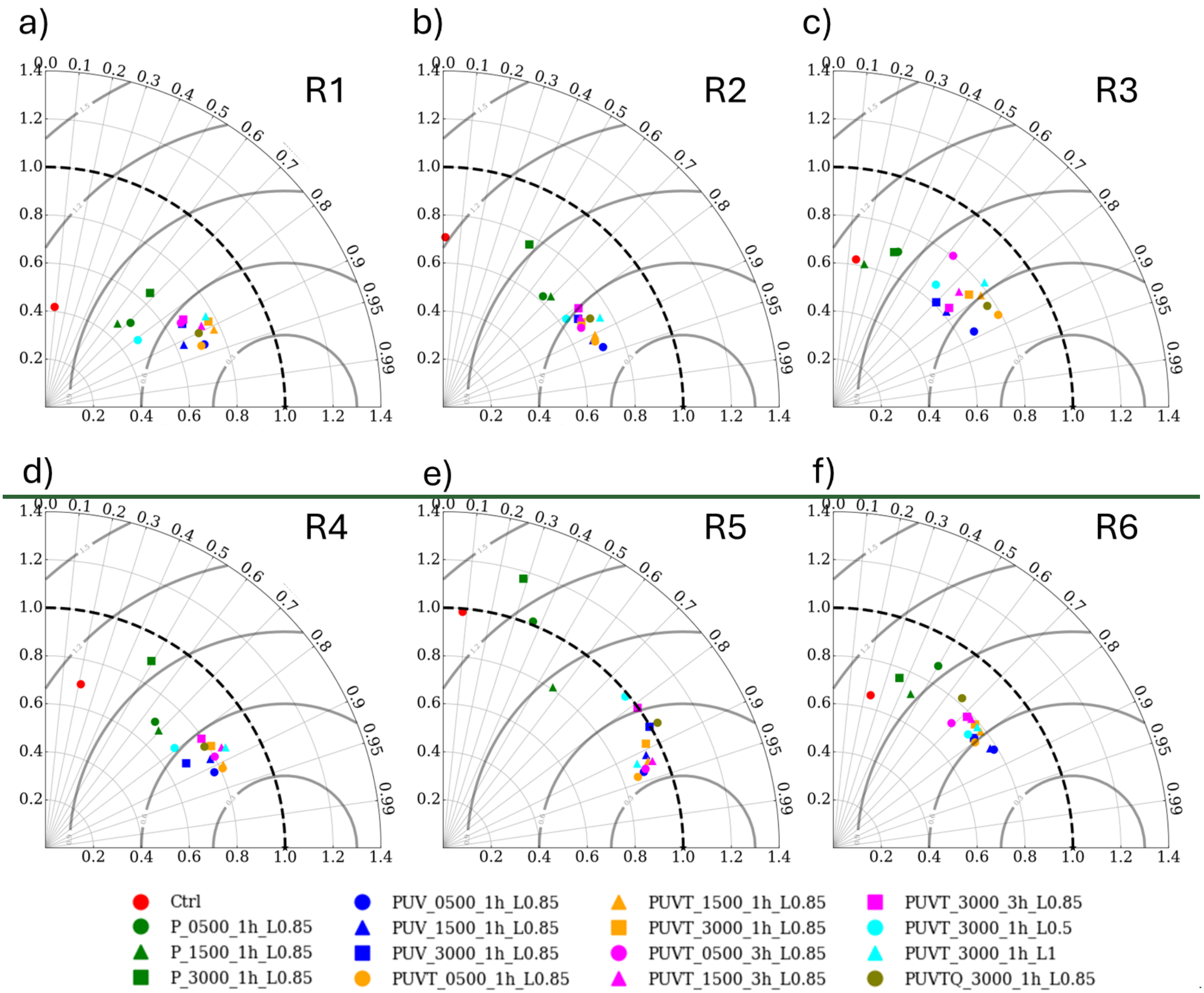
a)
R1
b)
R2
c)
R3
d)
R4
e)
R5
f)
R6
Ctrl
P_0500_1h_L0.85
P_1500_1h_L0.85
P_3000_1h_L0.85
PUV_0500_1h_L0.85
PUV_1500_1h_L0.85
PUV_3000_1h_L0.85
PUVT_0500_1h_L0.85
PUVT_1500_1h_L0.85
PUVT_3000_1h_L0.85
PUVT_0500_3h_L0.85
PUVT_1500_3h_L0.85
PUVT_3000_3h_L0.85
PUVT_3000_1h_L0.5
PUVT_3000_1h_L1
PUVTQ_3000_1h_L0.85

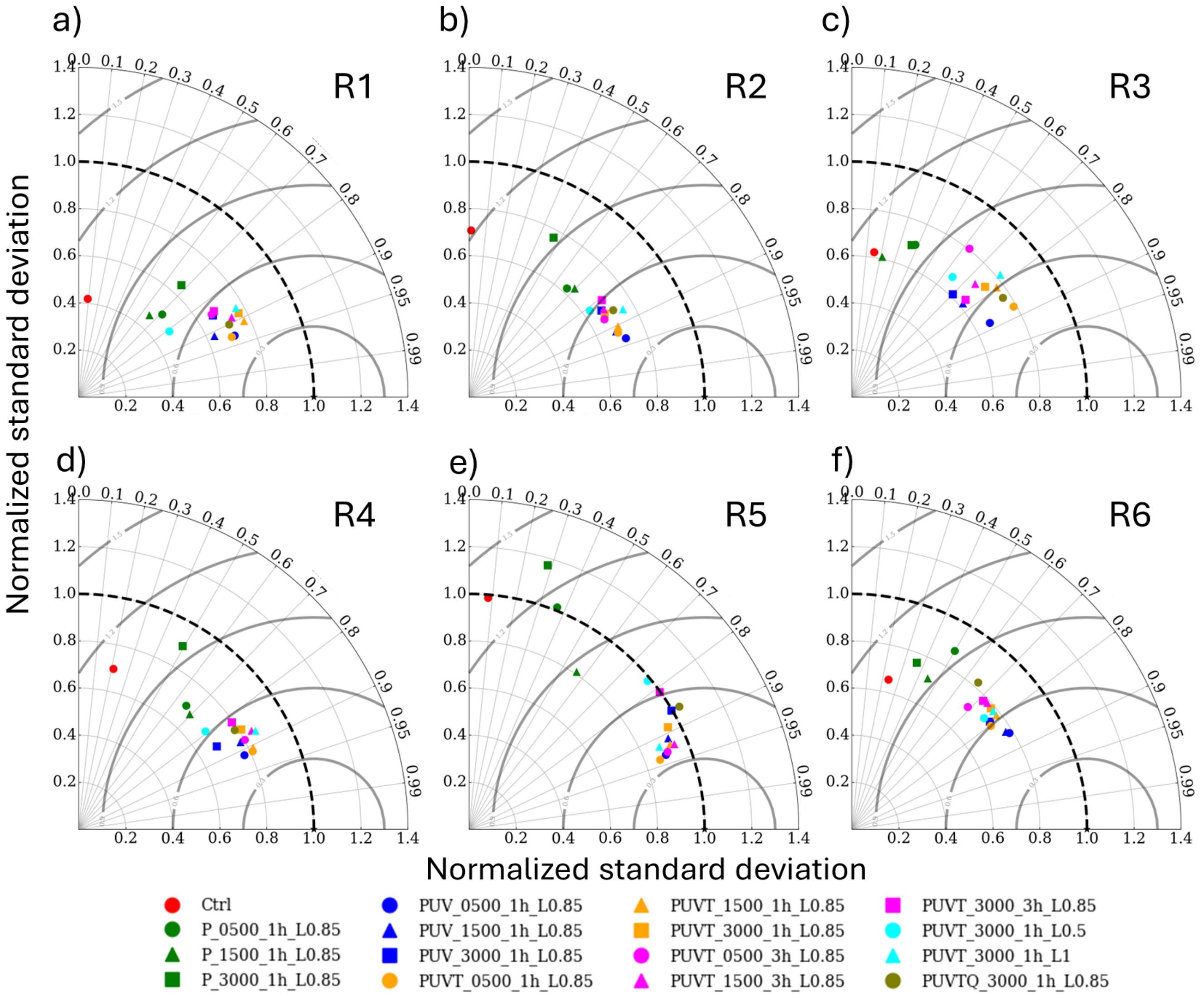

Figure 3 Taylor diagrams of daily precipitation averaged from December 2010 to March 2011 for six subregions (R1–R6), comparing 16 CCAM simulations with IMERG. Radial axis (distance from origin) represents standard deviation of the simulated precipitation (normalized by the observed standard deviation, IMERG). Angular axis (angle from x-axis) represents correlation coefficient between models and IMERG. Solid gray concentric arcs represent the c~~a~~entered root-mean-square error (RMSE) between the models and IMERG [a distance from the reference point on x-axis at (1,0)]. Coloured markers denote simulation groups (legend).

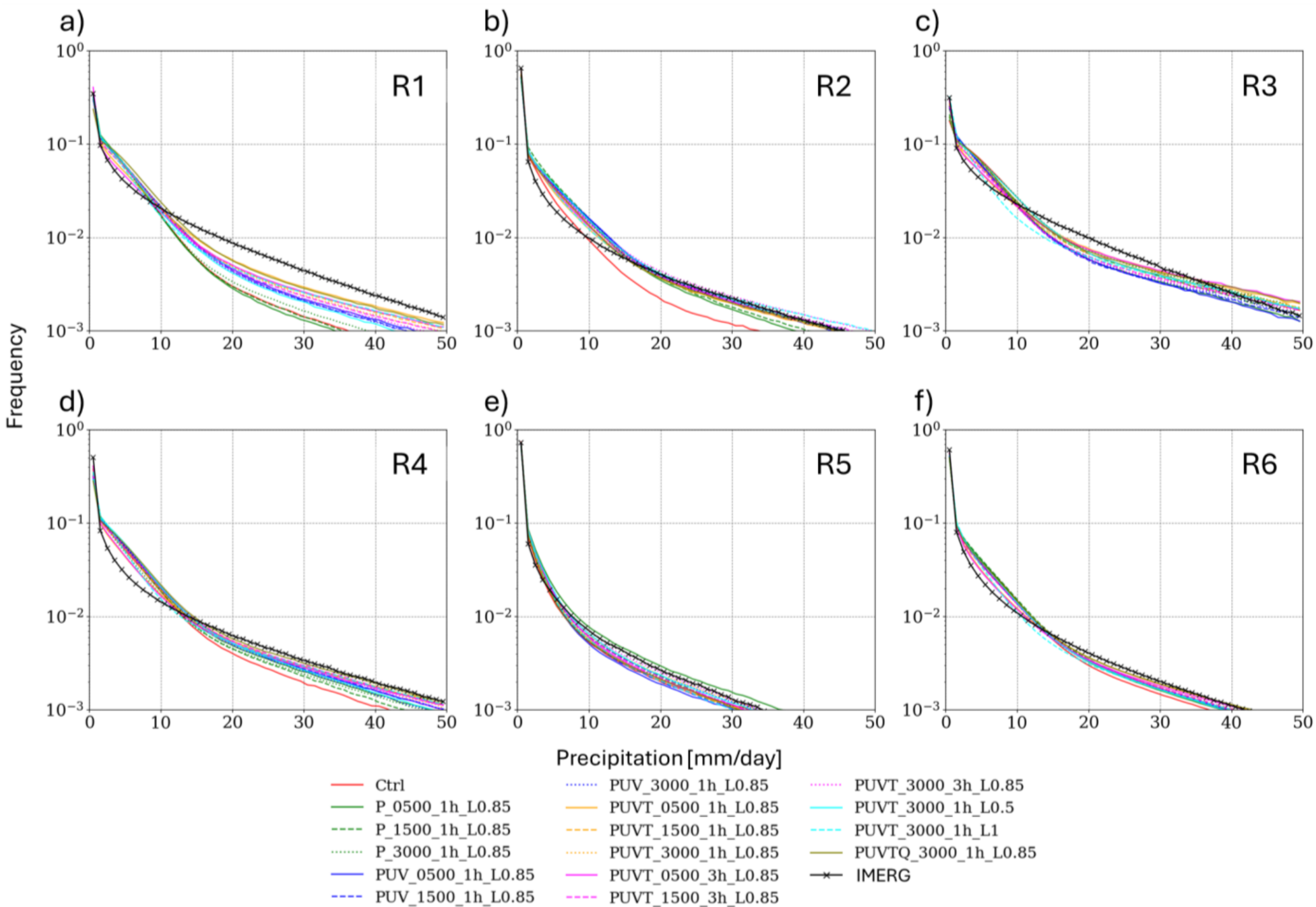

~~*Figure 4 Frequency of daily precipitation intensity for IMERG observation and 16 CCAM simulations averaged over each region from December 2010 to March 2011.*~~

We examined the frequency distributions of daily precipitation across six subregions (Fig. 4) to evaluate model fidelity relative to IMERG. All simulations overestimate (dashed red box) light precipitation (5 – 15 mm day^{-1}) and underestimate (dashed blue box) moderate events (15 – 30 mm day^{-1}), with the largest discrepancies in R1 and R3 (Figs. 4a and c). R5 is the only region where light-rainfall biases are minimal. The frequency of extremes (>40 mm day^{-1}) is reasonably reproduced across all simulations. Improvements from nudging are most evident in R2 and R4 in all nudged simulations. In contrast, light rain excess remains persistent in R1 and R3, underscoring the difficulty of correcting convective and orographic rainfall biases even under optimized nudging configurations.

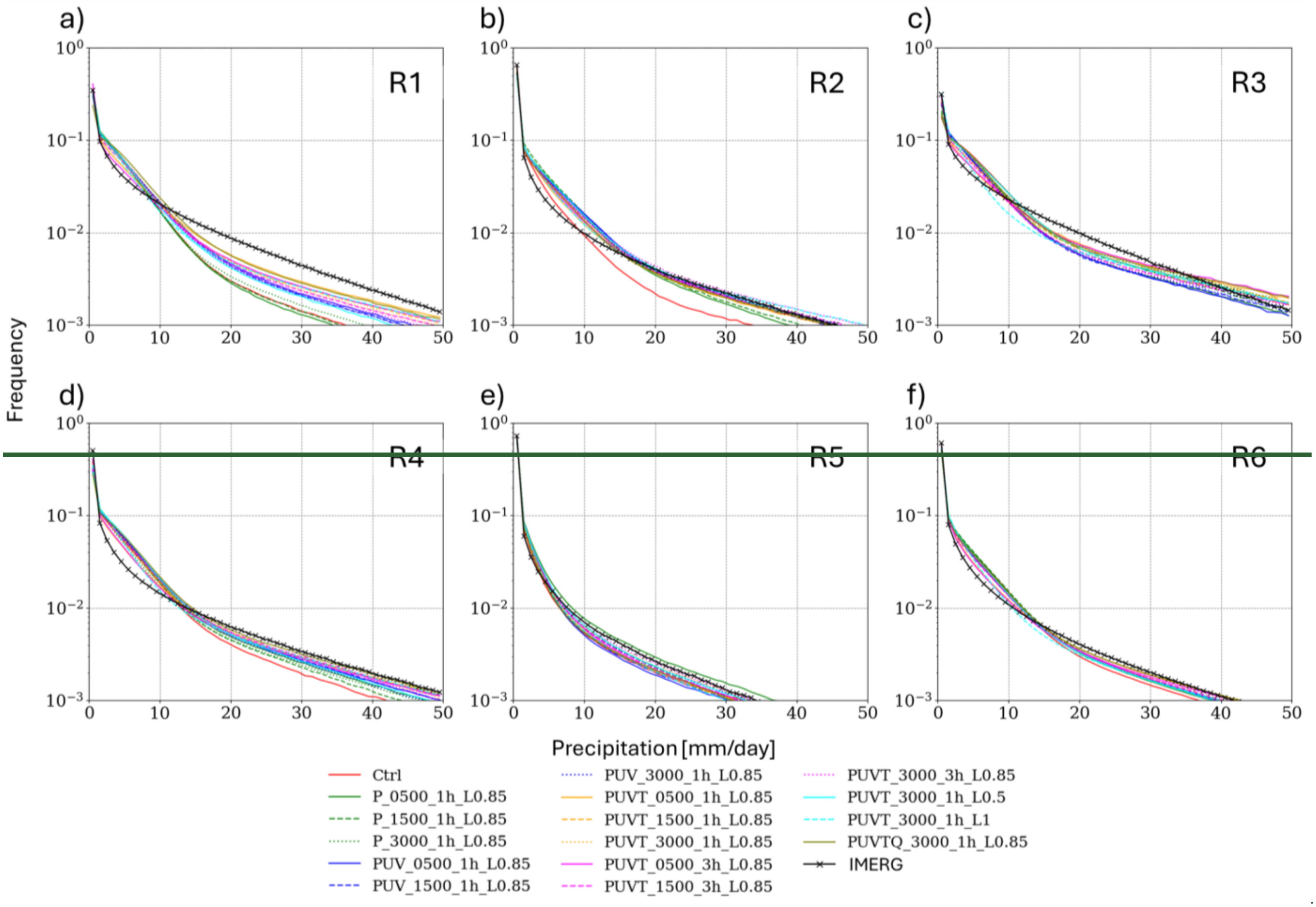

a)
R1
b)
R2
c)
R3
d)
R4
e)
R5
f)
R6
Frequency
Precipitation [mm/day]
Ctrl
P_0500_1h_L0.85
P_1500_1h_L0.85
P_3000_1h_L0.85
PUV_0500_1h_L0.85
PUV_1500_1h_L0.85
PUV_3000_1h_L0.85
PUVT_0500_1h_L0.85
PUVT_1500_1h_L0.85
PUVT_3000_1h_L0.85
PUVT_0500_3h_L0.85
PUVT_1500_3h_L0.85
PUVT_3000_3h_L0.85
PUVT_3000_1h_L0.5
PUVT_3000_1h_L1
PUVTQ_3000_1h_L0.85
IMERG

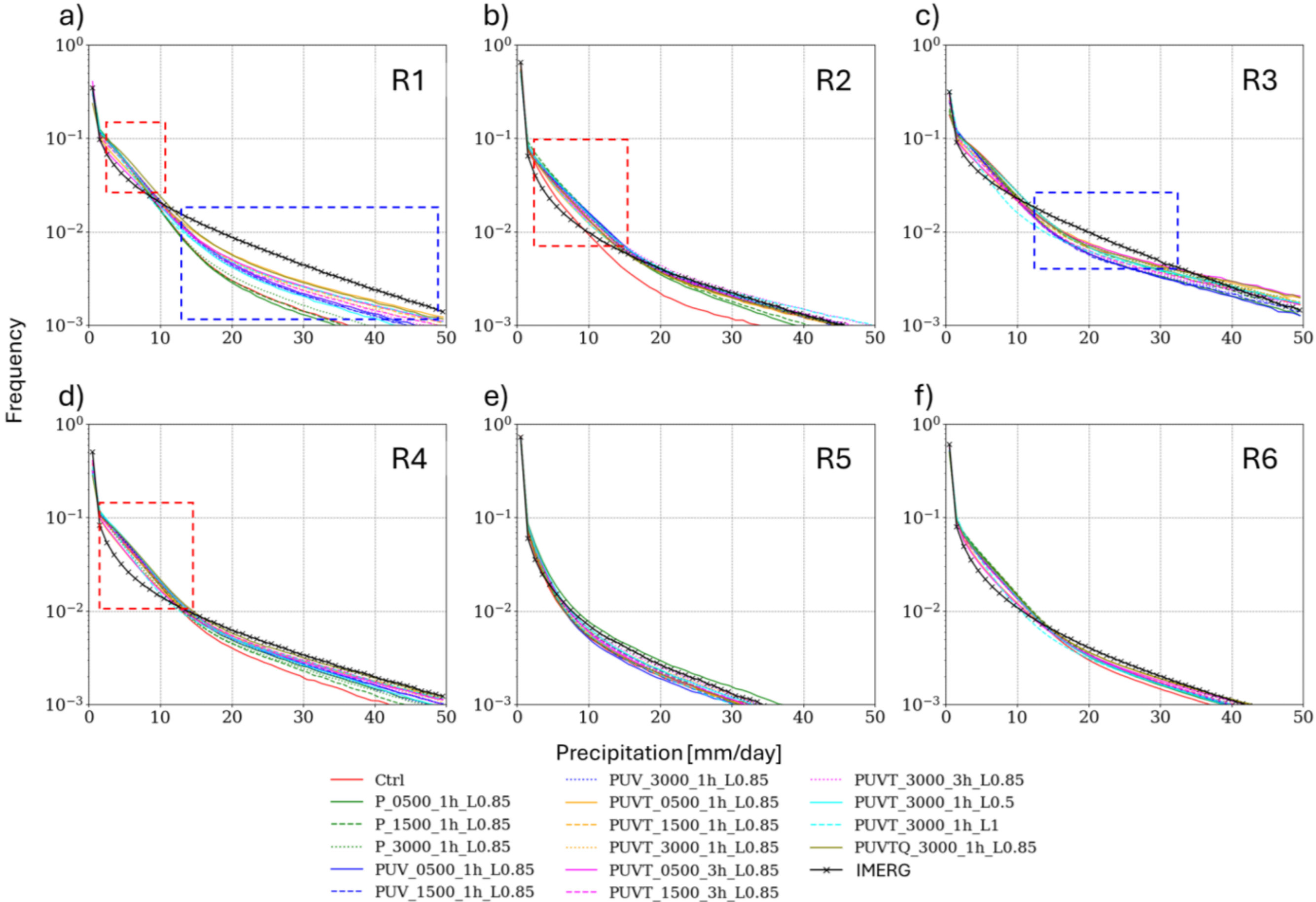

Figure 4 Frequency of daily precipitation intensity for IMERG ~~observation~~ and 16 CCAM simulations averaged over each region from December 2010 to March 2011. The dashed red and blue boxes indicate regions where the model respectively overestimates and underestimates precipitation compared to IMERG

3.1.2 Temporal variance of precipitation

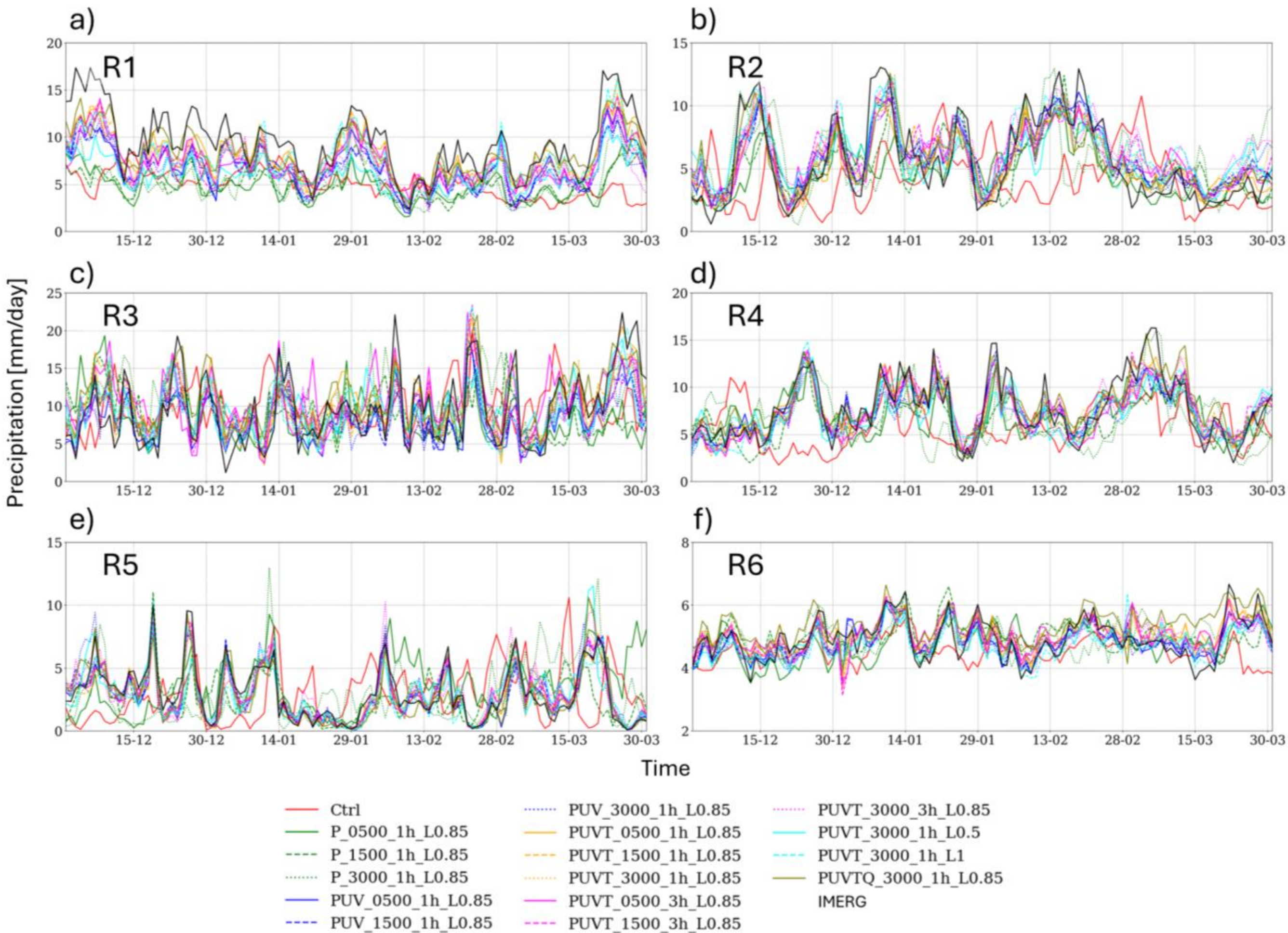

~~***Figure 5 Time series of spatially averaged daily rainfall (mm day^{-1}) for IMERG and 16 CCAM simulations over six from December 2010 to March 2011.***~~

Across all regions, the *Ctrl* simulation persistently underestimates rainfall (e.g., ~10 mm day⁻¹ deficit in R4 on 25 December 2010) while occasionally exaggerating daily peaks (e.g., >12 mm in R2 on 1 March 2011) (Fig. 5). It often fails to reproduce the timing of major events such as severe tropical cyclone Carlos over Darwin (15 February 2011, in Fig. 5b) and Yasi over Queensland (02 February 2011, in Fig. 5d). Nudged simulations substantially improve both timing and magnitude, reducing errors to ~1 – 5 mm day^{-1}. This is likely a result of nudging's ability to maintain large-scale atmospheric conditions, which allows the model to more accurately simulate the dynamics of tropical cyclones like Carlos and Yasi, thereby improving precipitation representation. Depending on nudging configurations, some runs (e.g., *P_1500_1h_L0.85*) slightly underestimate peak intensities by 1 – 2 mm day^{-1}. The largest improvements occur in R1 and R4, where *Ctrl* underestimates of ~10 mm day^{-1} are reduced to <1.5 mm day^{-1} in the best-performing *PUVT* runs, consistent with Taylor diagrams (Fig. 3) showing correlations rising from ~0.5 in the *Ctrl* to >0.9 with nudging. The persistent underestimation in R1 through the entire timeseries may partly reflect its lower horizontal resolution (e.g., > 20 km, Fig. 1) relative to IMERG.

The best overall performance is delivered by the *PUVT_1h* group at 500 – 1500 km with short update intervals (1h, L0.85), which closely track the IMERG time series in R1 – R4, correcting peak errors of 10 mm day^{-1} to <1.5 mm day^{-1} while maintaining realistic phase alignment of major synoptic events. Moderate skill is achieved by the *PUVT_3h* group and *PUV* runs, which improve timing and magnitude in some regions but degrade performance in others. In contrast, adding moisture or applying mid- or full-column nudging does not provide clear benefits, and in some cases degrades performance. The poorest outcomes are seen in the *Ctrl* and *P_var* groups, which either sustain exaggerated peaks (>15 mm day^{-1}) or distort the temporal structure.

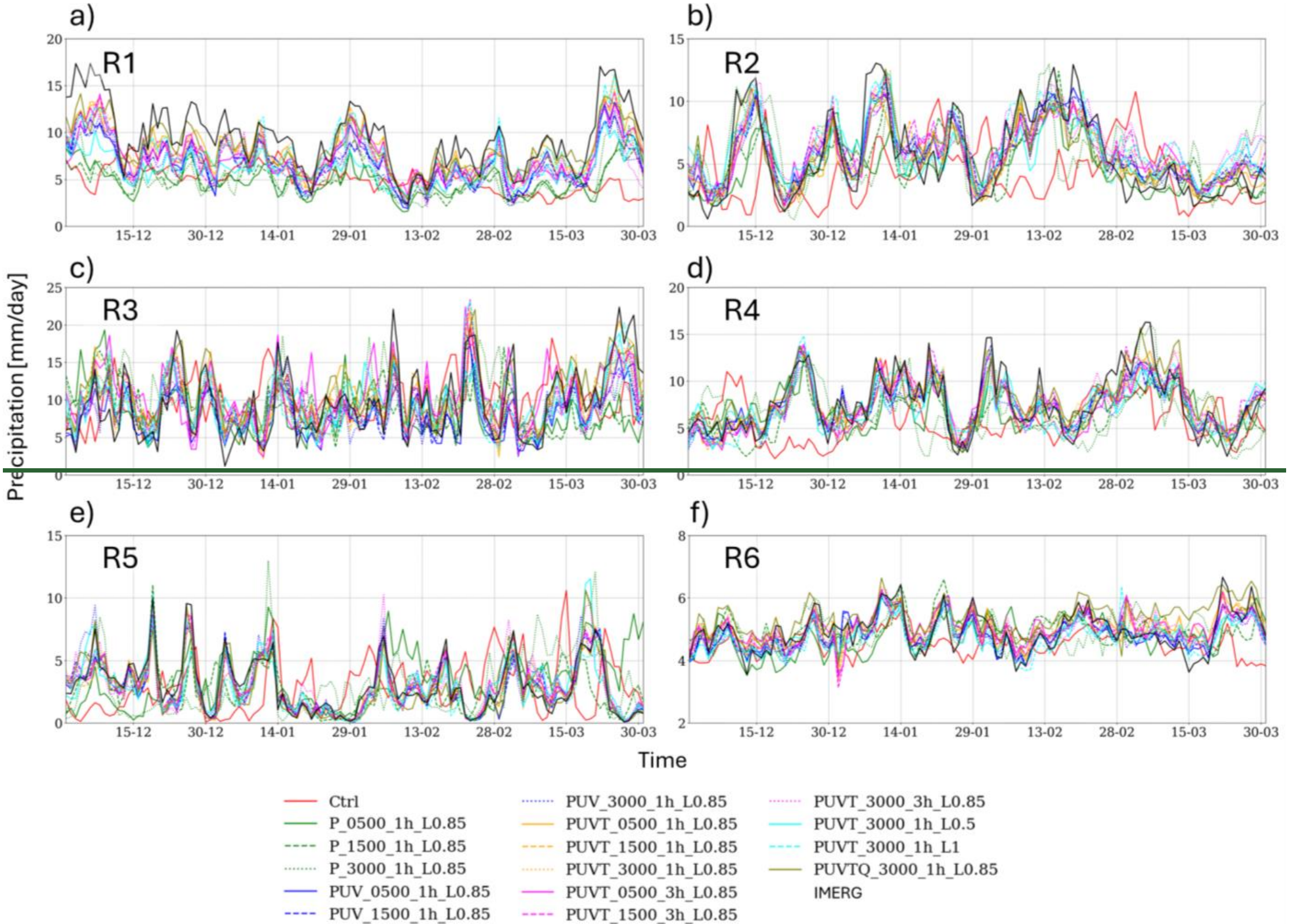
a)
R1
b)
R2
c)
R3
d)
R4
e)
R5
f)
R6
Precipitation [mm/day]
Time
15-12
30-12
14-01
29-01
13-02
28-02
15-03
30-03
Ctrl
P_0500_1h_L0.85
P_1500_1h_L0.85
P_3000_1h_L0.85
PUV_0500_1h_L0.85
PUV_1500_1h_L0.85
PUV_3000_1h_L0.85
PUVT_0500_1h_L0.85
PUVT_1500_1h_L0.85
PUVT_3000_1h_L0.85
PUVT_0500_3h_L0.85
PUVT_1500_3h_L0.85
PUVT_3000_3h_L0.85
PUVT_3000_1h_L0.5
PUVT_3000_1h_L1
PUVTQ_3000_1h_L0.85
IMERG

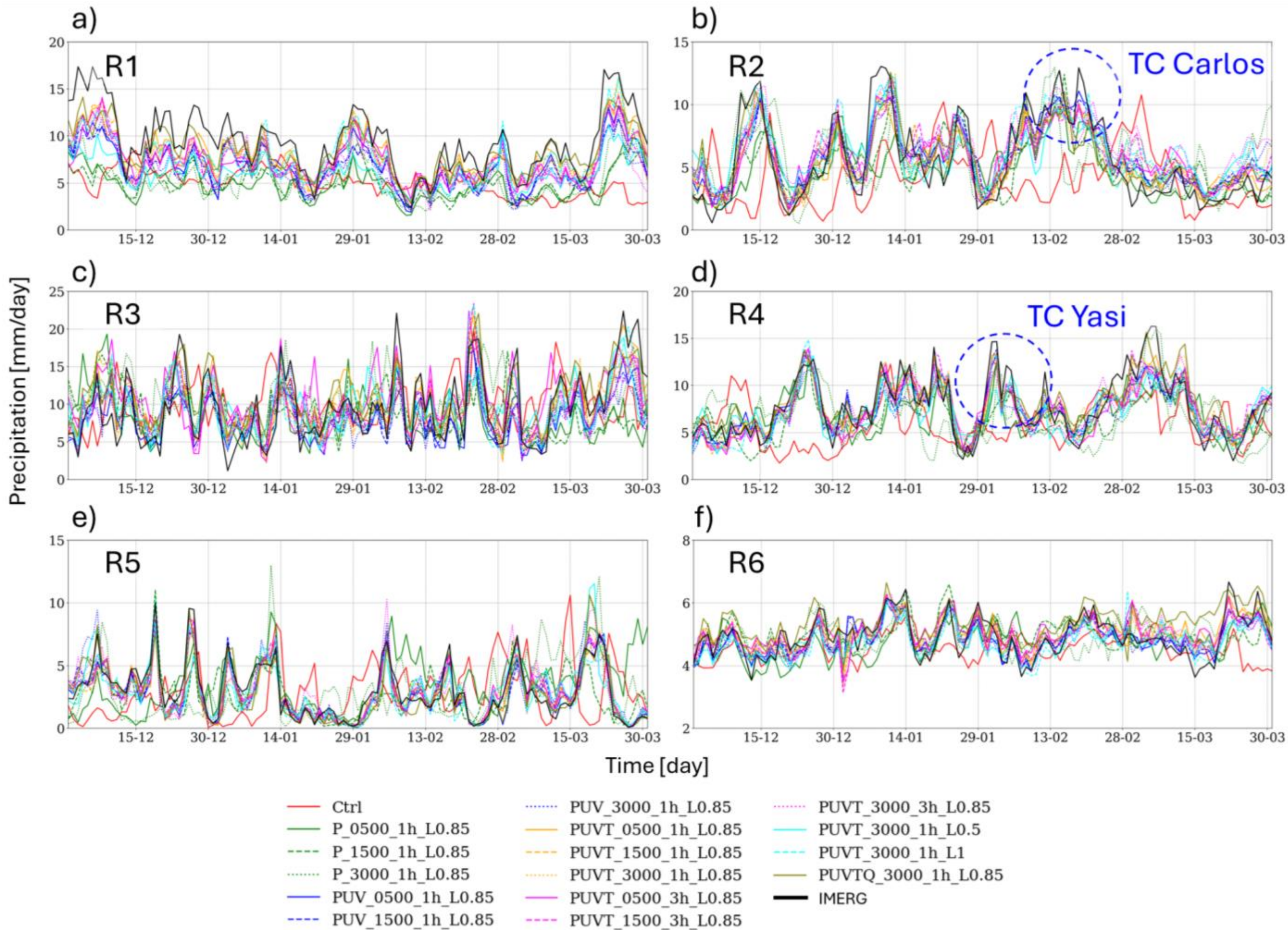

Figure 5 Time series of spatially averaged daily rainfall (mm day^{-1}) for IMERG and 16 CCAM simulations over the six from December 2010 to March 2011.

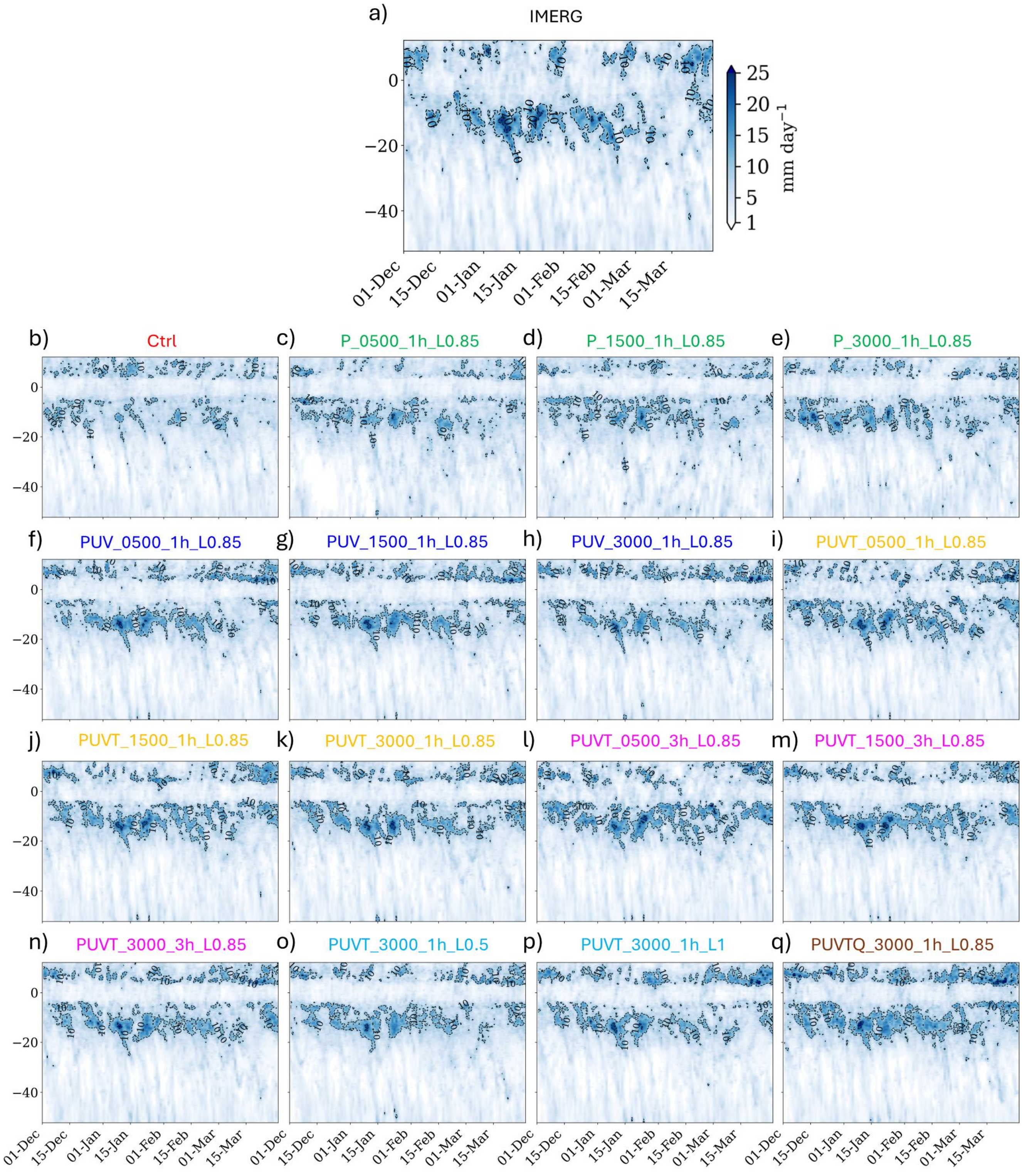
a) IMERG
mm day^{-1}
25
20
15
10
5
1
01-Dec
15-Dec
01-Jan
15-Jan
01-Feb
15-Feb
01-Mar
15-Mar
b) Ctrl
c) P_0500_1h_L0.85
d) P_1500_1h_L0.85
e) P_3000_1h_L0.85
f) PUV_0500_1h_L0.85
g) PUV_1500_1h_L0.85
h) PUV_3000_1h_L0.85
i) PUVT_0500_1h_L0.85
j) PUVT_1500_1h_L0.85
k) PUVT_3000_1h_L0.85
l) PUVT_0500_3h_L0.85
m) PUVT_1500_3h_L0.85
n) PUVT_3000_3h_L0.85
o) PUVT_3000_1h_L0.5
p) PUVT_3000_1h_L1
q) PUVTQ_3000_1h_L0.85

~~*Figure 6 Hovmöller diagram of zonally averaged daily precipitation (mm day^{-1}) from the IMERG dataset for the period 1 December 2010 to 31 March 2011, averaged over 90°E to 170°E.*~~

The Hovmöller diagram of zonally averaged daily precipitation (Fig. 6) highlights the dominant influence of the MJO on rainfall variability during December 2010 – March 2011. IMERG indicates persistent convective maxima within ~15°S – 15°N, punctuated by two strong episodes in mid-January and early February 2011 with daily zonal means exceeding 25 mm day^{-1} (Fig. 6a). These surges coincide with active MJO phases over the MC and western Pacific (RMM phases 4 – 7) (Fig. S5), consistent with the enhanced precipitation in the regional time series (Fig. 5) for R1–R4. However, the *Ctrl* fails to reproduce the intensity and spatial coherence of these convective maxima (dashed red box, Fig. 6b). Precipitation within 15°S–15°N is markedly weaker, with zonal means rarely exceeding 10 mm day^{-1}, and both major MJO surges are substantially underestimated. Convective regions appear fragmented and displaced, indicating the model's inability to capture the organized eastward propagation of MJO. South of 20°S, rainfall is sporadic and lacks the intensity and persistence evident in IMERG, consistent with the dry biases in the regional time series (Fig. 5). Collectively, these deficiencies demonstrate the *Ctrl*'s limited skill in representing tropical intraseasonal variability and its teleconnections across the MC and Australasian domain.

Nudged simulations markedly improve the zonal-mean representation of tropical precipitation compared to the *Ctrl* (Fig. 6c-q). Across most configurations, convective maxima within 15°S – 15°N are intensified and better aligned with the MJO-related surges in mid-January and early February 2011, reducing the dry bias evident in the *Ctrl*. The *PUVT_1h* group at short wavelengths (e.g., 500 – 1500 km, Fig. 6) perform best, capturing both the magnitude and spatial coherence of the convective regions and closely tracking the eastward propagation of MJO. *PUV* and *PUVT_3h* runs also provide noticeable improvements in timing and magnitude, though their maxima are somewhat weaker than observed. Furthermore, configurations with mid-column nudging degrades model performance to represent MJO (Fig. 6o) whereas nudging from the surface to the top of the atmosphere does not add further benefit compared to other *PUVT* nudged simulations (Fig. 6p). The inclusion of specific humidity exaggerates light rainfall while failing to represent the organized MJO surges (Fig. 6q).

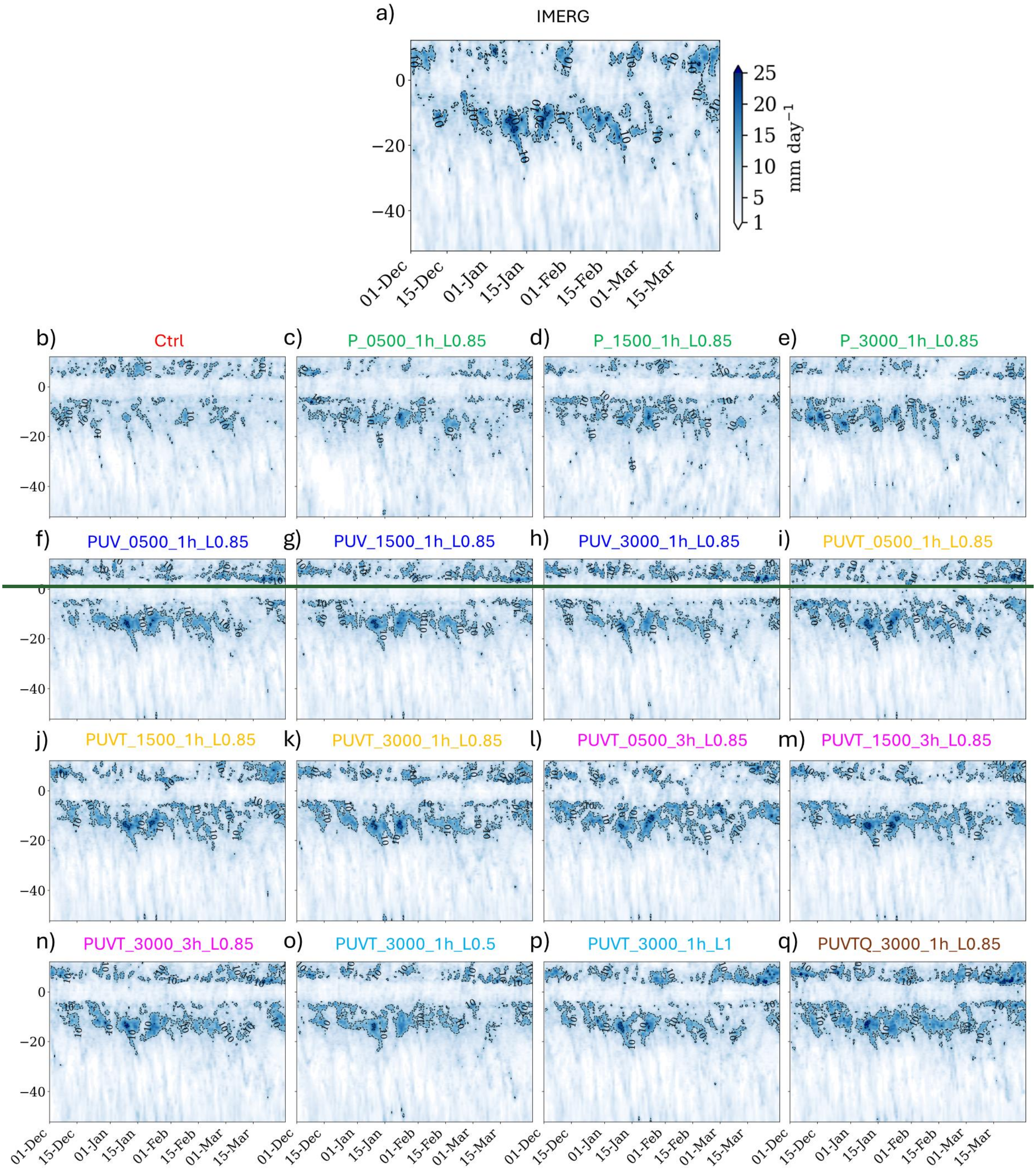

a)
IMERG
mm day^{-1}
b) Ctrl
c) P_0500_1h_L0.85
d) P_1500_1h_L0.85
e) P_3000_1h_L0.85
f) PUV_0500_1h_L0.85
g) PUV_1500_1h_L0.85
h) PUV_3000_1h_L0.85
i) PUVT_0500_1h_L0.85
j) PUVT_1500_1h_L0.85
k) PUVT_3000_1h_L0.85
l) PUVT_0500_3h_L0.85
m) PUVT_1500_3h_L0.85
n) PUVT_3000_3h_L0.85
o) PUVT_3000_1h_L0.5
p) PUVT_3000_1h_L1
q) PUVTQ_3000_1h_L0.85
01-Dec
15-Dec
01-Jan
15-Jan
01-Feb
15-Feb
01-Mar
15-Mar

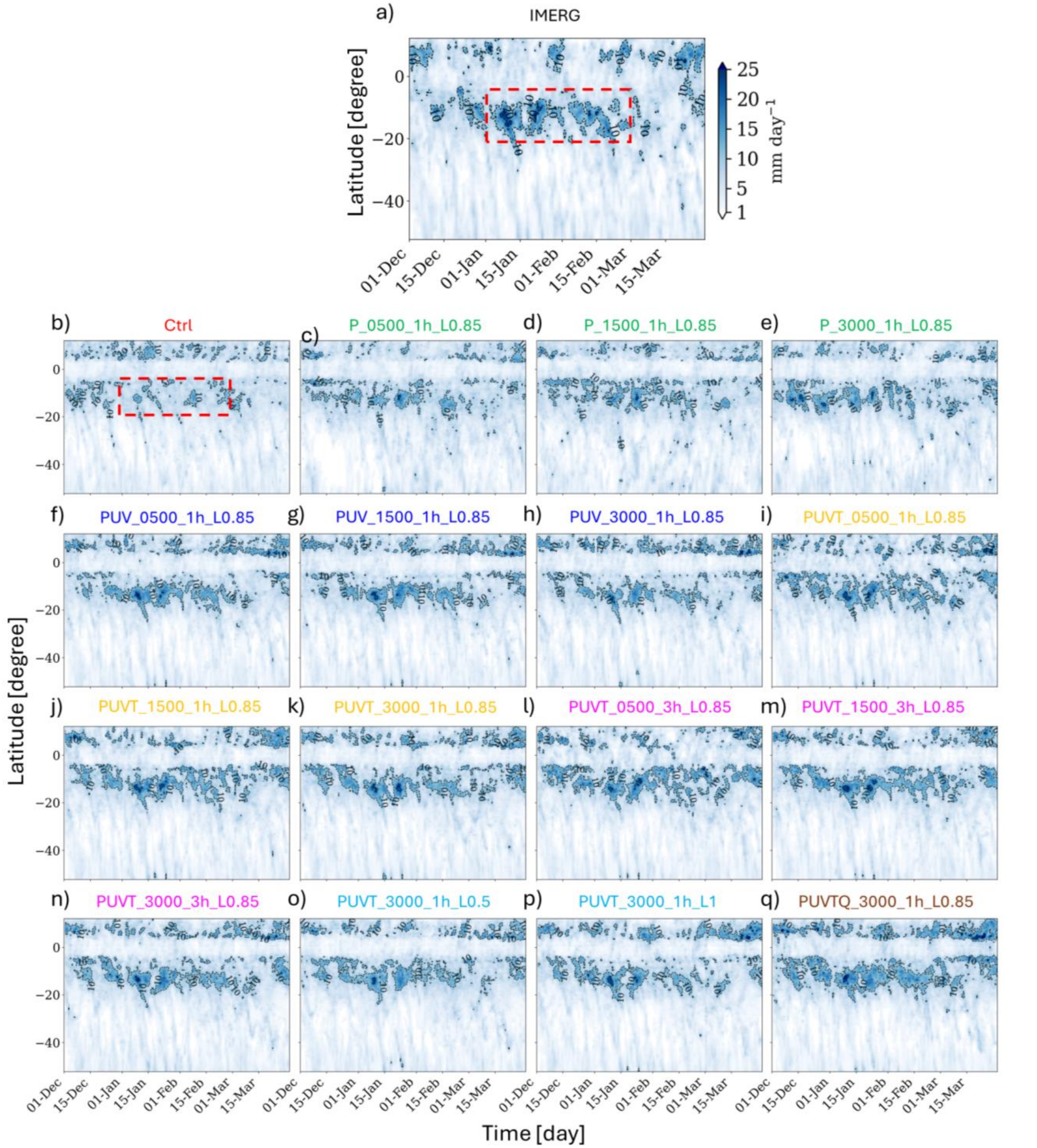

425

Figure 6 Hovmöller diagram of zonally averaged daily precipitation (mm day^{-1}) from the IMERG dataset for the period 1 December 2010 to 31 March 2011, averaged over 90°E to 170°E. Dash red box indicates the regions of MJO-related peak precipitation.

3.1.3 Low-level circulation and vertical correlation

The analysis of moisture flux divergence from ERA5 data (Fig. 7) reveals distinct spatial patterns during the 2010 – 2011 La Niña event. A prominent convergence zone (blue shading) is observed over northern and northwest Australia (Fig. 7a), closely aligned with the low-pressure system in this region (Fig. ~~S6~~S7). Subtropical divergence (red shading) south of approximately 30°S reflects subsidence, associated with a high-pressure system to the south (Fig. ~~S6~~S7), which likely contributes to suppressed rainfall over southern Australia, consistent with the observed decrease in precipitation shown in Fig. 1a. Low-level wind patterns indicate monsoonal winds from the tropics, driving moisture towards the Australian continent, a feature consistent with the active Australian monsoon during this period (e.g., BoM, 2012; Giles, 2012; Lisonbee and Ribbe 2021). The convergence regions identified in Fig. 7a qualitatively correspond to high-precipitation areas, particularly over the Gulf of Carpentaria, west of Sumatra, New Guinea, the MC, and New Zealand (Fig. 1a). In contrast, the *Ctrl* exhibits a weaker and displaced low-pressure system over northwest Australia, resulting in diminished moisture convergence and an underestimation of precipitation in those regions such as the Gulf of Carpentaria, as seen in Fig. 1a. These discrepancies highlight the limitations of the *Ctrl* in accurately capturing monsoonal dynamics. In contrast, the nudged simulations significantly improve both the spatial structure and magnitude of moisture convergence, as well as the low-level circulation. The inclusion of pressure nudging (Fig. 7c~~-e~~) enhances the representation of low- and high-pressure systems over Australia, with the low-pressure system over northwest Australia becoming more defined and accurately positioned relative to the *Ctrl*. ~~The inclusion of *u* and *v* wind~~ Wind nudging (*u* and *v*) in *PUV* (Fig. 7d~~f-h~~) ~~and *PUVT* (Fig. 7i-n)~~ simulations ~~greatly~~ enhances monsoonal wind flow towards Australia, improving moisture convergence in regions such as the Gulf of Carpentaria and New Guinea, and aligning moisture flux divergence more closely with observed precipitation patterns~~, especially at shorter wavelengths (e.g., PUVT_0500_1h_L0.85 and PUVT_1500_1h_L0.85).~~. This also improves MJO phase dynamics, ensuring the precipitation peak occurs in the correct location (Fig. 5f-h). Additionally, the inclusion of temperature nudging *PUVT* (Fig. 7e) further refines the MJO-related precipitation peak, reproducing it more comparable to IMERG (Fig. 5i-n). Quantitatively, the location and magnitude of convergence regions over northern Australia improve by ~30 – 40% compared to the *Ctrl*. ~~It is important to note that nudging is not applied below 850 hPa, except for in the *PUVT_3000_1h_L1* case; however, similar improvements in moisture transport and convergence are observed at 875 hPa.~~ Similar improvements in moisture transport and convergence in Fig. 7 are also observed at both lower (e.g., 900 hPa) and upper levels (e.g., 800 hPa). There is minimal difference ~~in moisture transport and convergence~~ between ~~cases~~ simulations where nudging is applied from 500 hPa (mid-troposphere to top of the atmosphere)~~ and from the surface to the top of the atmosphere~~. However, ~~when~~ moisture nudging ~~is included,~~introduced additional convergence regions emerge, particularly over northern ~~and western~~ Australia, ~~which corresponds to the~~leading to overestimated rainfall ~~(observed in~~ Fig. 5f, ~~and~~ 6q and Fig. 7g). This underperformance could be partly due to biases in ERA5 moisture fields, especially in regions with sparse observations, which introduce uncertainties and limit the effectiveness of nudging in improving precipitation simulations (Virman et al., 2021; Truong et al., 2022).

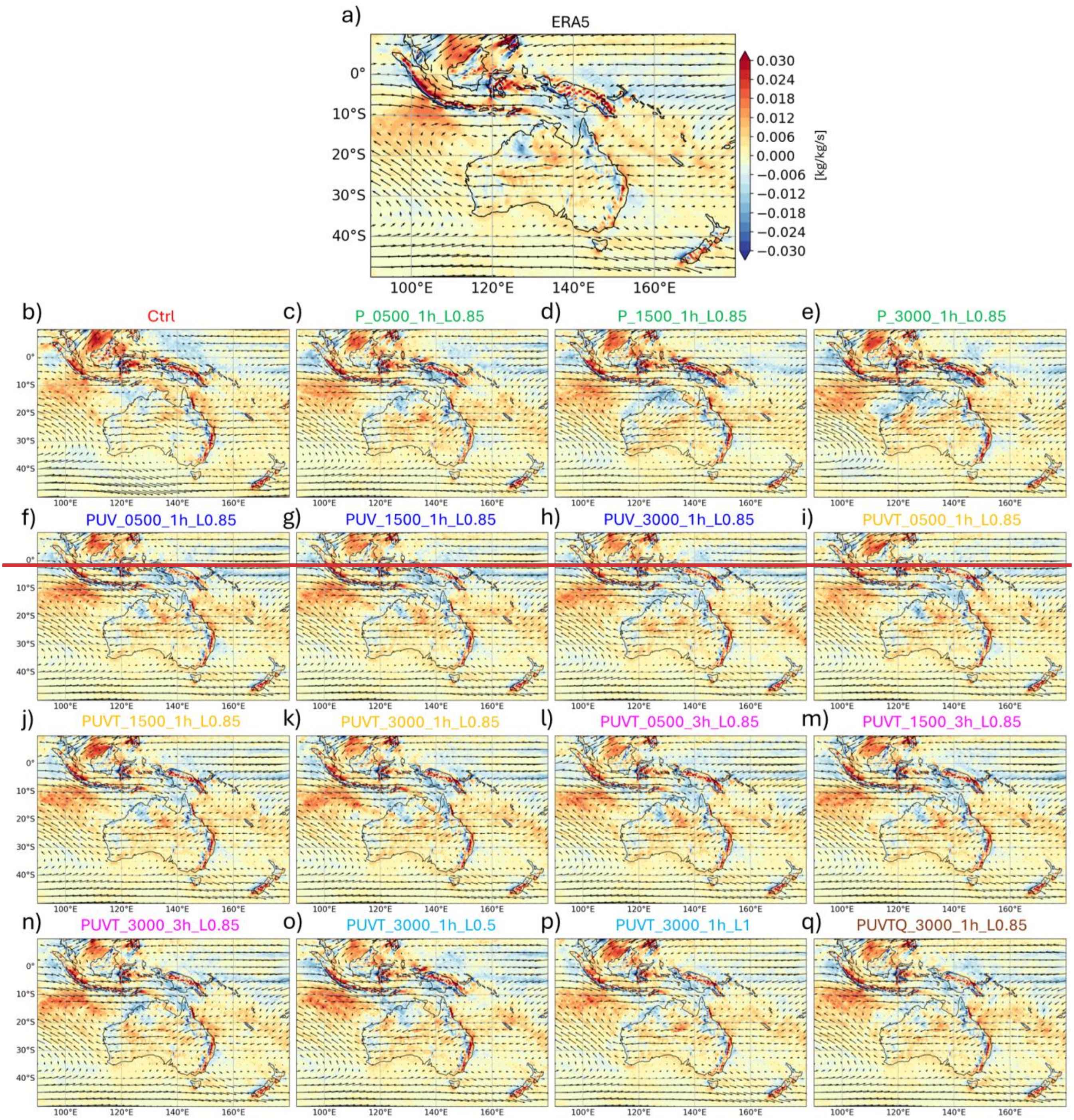
a)
ERA5
[kg/kg/s]
0.030
0.024
0.018
0.012
0.006
0.000
−0.006
−0.012
−0.018
−0.024
−0.030
0°
10°S
20°S
30°S
40°S
100°E
120°E
140°E
160°E
b) Ctrl
c) P_0500_1h_L0.85
d) P_1500_1h_L0.85
e) P_3000_1h_L0.85
f) PUV_0500_1h_L0.85
g) PUV_1500_1h_L0.85
h) PUV_3000_1h_L0.85
i) PUVT_0500_1h_L0.85
j) PUVT_1500_1h_L0.85
k) PUVT_3000_1h_L0.85
l) PUVT_0500_3h_L0.85
m) PUVT_1500_3h_L0.85
n) PUVT_3000_3h_L0.85
o) PUVT_3000_1h_L0.5
p) PUVT_3000_1h_L1
q) PUVTQ_3000_1h_L0.85

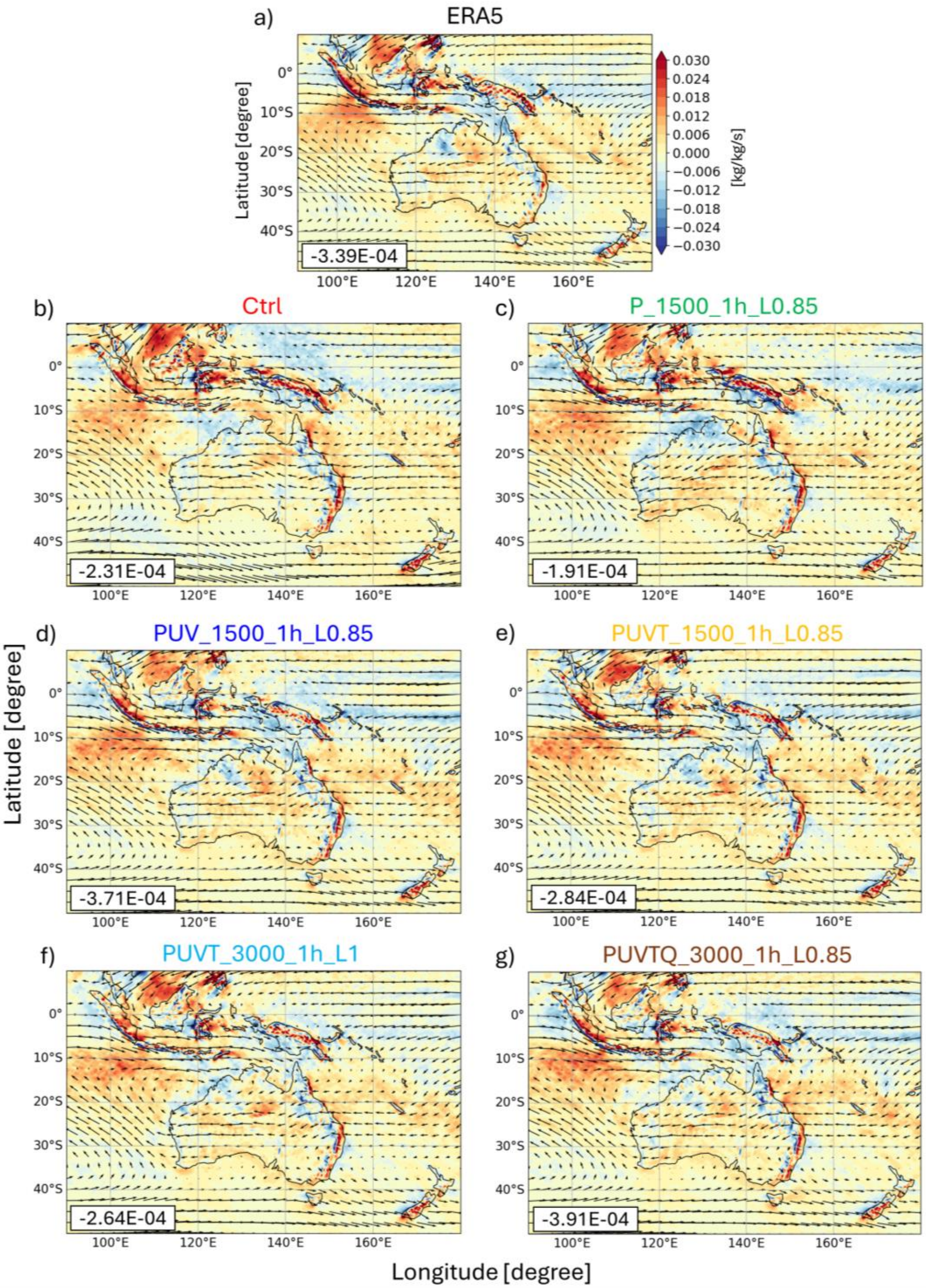

465 ***Figure 7 The averaged wind fields (vectors) and water vapor flux divergence (colour shades; unit) from ERA5 at 875 hPa from December 2010 to March 2011 over study domain; (a) ERA5 and (b)–(q) the corresponding plot for the 16 CCAM simulations. Black boxes in the lower left of each panel indicate the domain averaged values.***

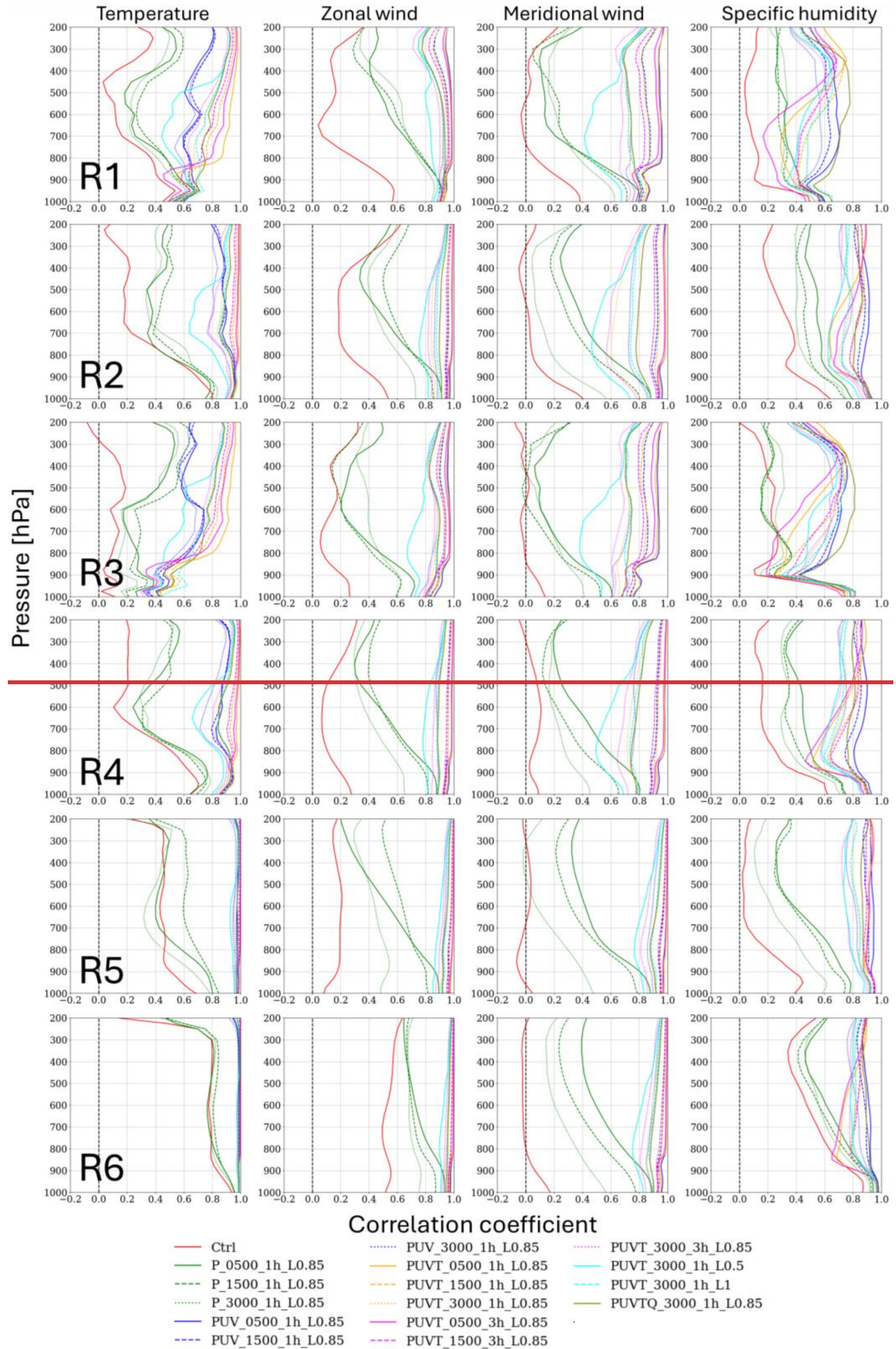

Temperature
Zonal wind
Meridional wind
Specific humidity
R1
R2
R3
R4
R5
R6
Pressure [hPa]
Correlation coefficient
Ctrl
P_0500_1h_L0.85
P_1500_1h_L0.85
P_3000_1h_L0.85
PUV_0500_1h_L0.85
PUV_1500_1h_L0.85
PUV_3000_1h_L0.85
PUVT_0500_1h_L0.85
PUVT_1500_1h_L0.85
PUVT_3000_1h_L0.85
PUVT_0500_3h_L0.85
PUVT_1500_3h_L0.85
PUVT_3000_3h_L0.85
PUVT_3000_1h_L0.5
PUVT_3000_1h_L1
PUVTQ_3000_1h_L0.85

~~*Figure 8 Vertical profiles of the correlation coefficient for the spatial pattern of Temperature, U wind component, V wind component, specific humidity from top to bottom 16 CCAM simulations against ERA from December 2010 to March 2011 over 6 regions R1 to R6 from left to right.*~~

Figure 8 presents vertical correlations of temperature (*t*), zonal wind (*u*), meridional wind (*v*), and specific humidity (*q*) between 16 CCAM simulations and ERA5 across the six subregions (R1 – R6). The *Ctrl* run exhibits the weakest skill, with correlations frequently below 0.4 in the mid- to upper troposphere (400–200 hPa). Nudged simulations markedly improve vertical coherence, although the magnitude of improvement varies by configurations. For temperature, the *PUVT_1h* group, particularly, *PUVT_0500_1h_L0.85* and *PUVT_1500_1h_L0.85* simulations achieve correlations exceeding 0.8, whereas mid-column nudging (*PUVT_3000_1h_L0.5*) ~~—~~degrades the simulated temperature skill and full-column nudging (*PUVT_3000_1h_L1*) offers no additional benefit, reinforcing the concept of constraining above the boundary layer while allowing near-surface fields to evolve freely. For winds, correlations in the *Ctrl* remain weak (<0.5) throughout much of the troposphere, consistent with its poor representation of monsoon inflow and subtropical divergence (Fig. 7b). Nudged simulations, particularly *PUV* and *PUVT* at 500 – 1500 km, raise correlations to 0.7 – 0.9 across most levels, although values remain lower in the upper troposphere over R1 and R3. Specific humidity shows the greatest variability. In the *Ctrl*, correlations drop largely above 700 hPa (<0.2 in R1–R3), while *PUVT_0500_1h_L0.85* and *PUVT_1500_1h_L0.85* improve to 0.6 – 0.8 in the mid-troposphere. Although nudging moisture (*PUVTQ_3000_1h_L0.85*) enhances the simulated specific humidity, the correlation does not differ significantly from other nudged simulations that do not include moisture nudging (Fig. 8). The correlation in specific humidity over region R3 between all models and ERA5 is lower at 900 hPa (Fig. 8), indicating spatial variability with regions both too dry and too wet, which reduces correlation (Fig. S8). At 975 hPa, the correlation is higher, indicating less variability, with the model's systematic bias (over- or underprediction) aligning with ERA5, despite differing magnitudes (Fig. S8).

Regionally, R1 and R3 remain problematic even with nudging, as the vertical correlations for temperature and specific humidity in near the surface and aloft remain weaker, consistent with persistent rainfall biases (Fig. 2, 4). By contrast, R4 and R5 show the largest improvement across all four variables (Fig. 8), aligning with improved magnitude and event timing of precipitation in Figs. 5–6. Domain-wide vertical correlation (R6, rightmost in Fig. 8) further suggests that nudged runs consistently outperforming the *Ctrl* across all variables.

495

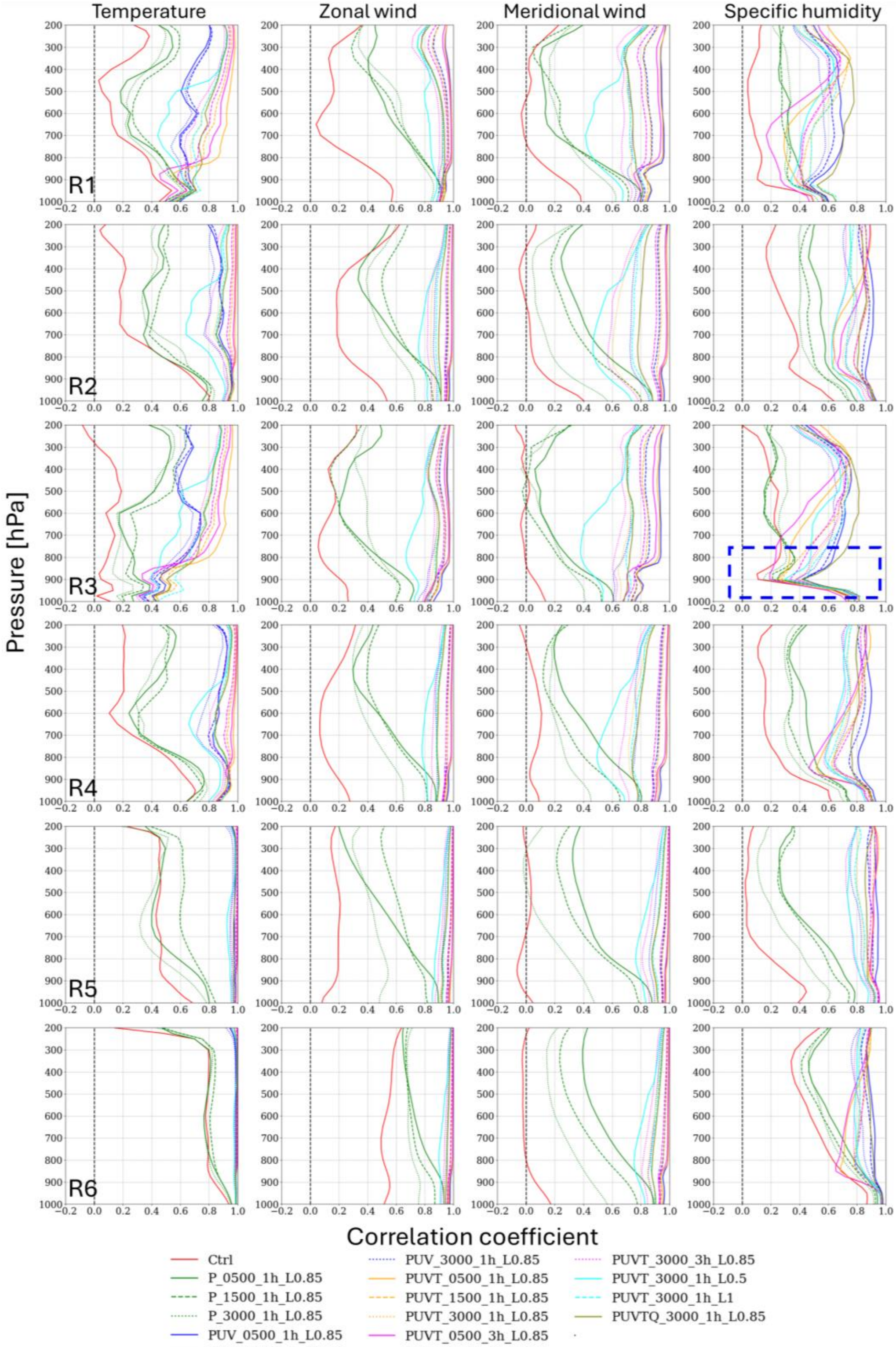
Temperature
Zonal wind
Meridional wind
Specific humidity
R1
R2
R3
R4
R5
R6
Pressure [hPa]
Correlation coefficient
Ctrl
P_0500_1h_L0.85
P_1500_1h_L0.85
P_3000_1h_L0.85
PUV_0500_1h_L0.85
PUV_1500_1h_L0.85
PUV_3000_1h_L0.85
PUVT_0500_1h_L0.85
PUVT_1500_1h_L0.85
PUVT_3000_1h_L0.85
PUVT_0500_3h_L0.85
PUVT_1500_3h_L0.85
PUVT_3000_3h_L0.85
PUVT_3000_1h_L0.5
PUVT_3000_1h_L1
PUVTQ_3000_1h_L0.85

Figure 8 Vertical profiles of the correlation coefficient for the spatial pattern of Temperature, U wind component, V wind component, specific humidity from top to bottom 16 CCAM simulations against ERA5 from December 2010 to March 2011 over 6 regions R1 to R6 from left to right.

3.2 Extreme precipitation

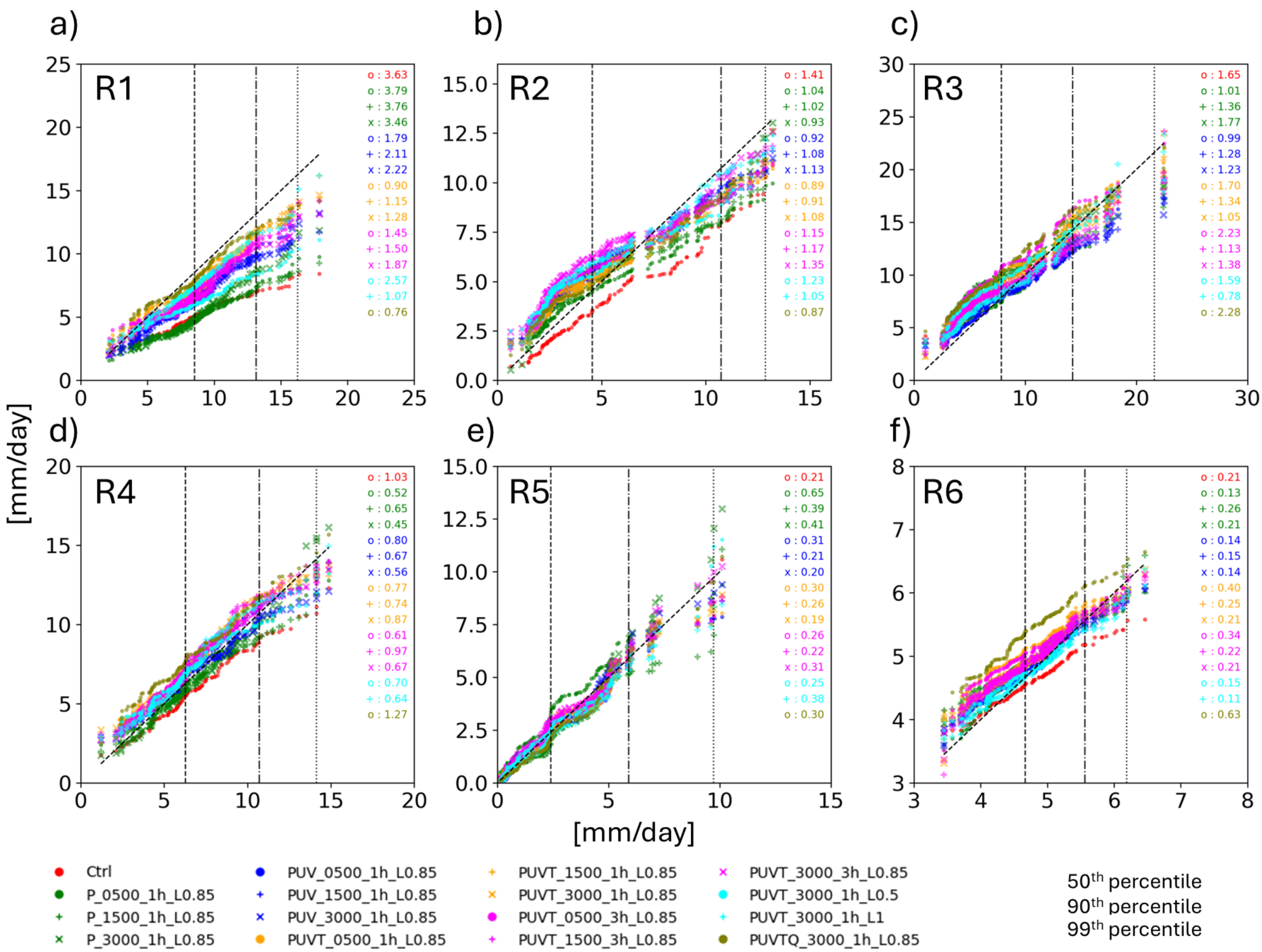

~~*Figure 9 Quantile–quantile plots of regionally averaged daily precipitation (mm day^{-1}) against IMERG for six subregions. Coloured symbols denote different CCAM simulations (see legend). The dashed 1:1 line represents perfect agreement with observations. The numbers indicate the area formed by the 1:1 and model line. Numbers on the top right of each panel indicate the area between IMERG and CCAM in which the larger the number the larger difference between the two.*~~

Figure 8 shows quantile – quantile (QQ) plots of daily regionally averaged precipitation against IMERG for the six subregions. The *Ctrl* shows the largest departures from the 1:1 line, systematically underestimating rainfall beyond the median (50th percentile) and failing to capture heavy rainfall above the 99th percentile in most regions, particularly R1, R2, R4, and whole domain, R6, consistent with its dry biases observed in Figs. 2 and 6. Nudged simulations substantially improves the precipitation distribution, with the best agreement achieved by *PUVT_1h* group (orange marker in Fig. 9). These configurations reduce mean biases to < 1 mm/day across all regions and closely follows IMERG up to the 90th percentile, while also reproducing the upper tail of the distribution (99th) more realistically, including the balance of extremes in R2-R5. It also stands out to be the best configuration for R1 region despite the coarse horizontal resolution. *PUVT_3h* group performs nearly as well, though with slightly scatter beyond the 90th percentile. It is interesting to note that the shorter wavelength (e.g., 500 and 1500 km) runs reduce biases substantially and follow IMERG closely through the 90th percentile, remaining stable without under- or overshooting. In contrast, longer-wavelength configurations (e.g., 3000 km) remain acceptable up to the 90th percentile but tend to under- or overshoot high-quantile rainfall thereafter, particularly in R3, R4, and R5, with normalized biases of ~3 – 5 mm/day. In contrast, moisture nudging (*PUVTQ_3000_1h_L0.85*) shows the largest biases, significantly increases rainfall above all percentiles (Fig. 9f). This is consistent with its degraded frequency distributions (Fig. 4f) and overestimation of zonally averaged daily precipitation (Fig. 6q). A persistent limitation across all simulations is the underestimation of the very highest extremes (above the 99.9th percentile) in R1 and R3, even in the best *PUVT* runs, reflecting unresolved convective and orographic processes. Overall, these diagnostics confirm that low-level, high-frequency *PUVT* nudging at intermediate wavelengths (500 – 1500 km, L0.85) provides the most balanced performance, reducing systematic biases across the distribution, from the median through the 90th percentile, while preserving realistic variability at higher quantiles whereas weaker (e.g., only pressure nudging) or over-constrained configurations (e.g., adding moisture) either fail to correct or exacerbate extremes.

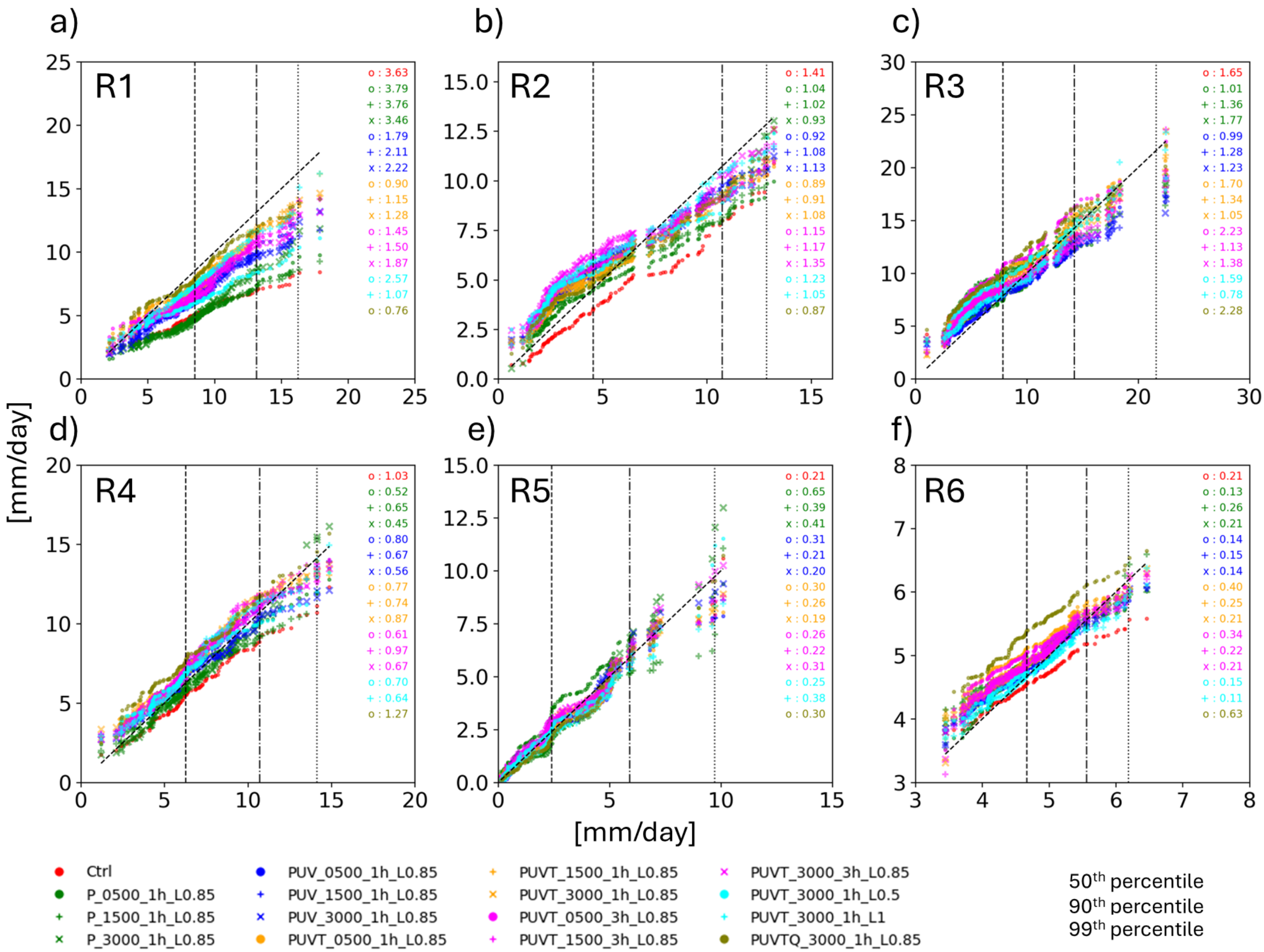

Figure 9 Quantile–quantile plots of regionally averaged daily precipitation (mm day⁻¹) against IMERG for six subregions. Coloured symbols denote different CCAM simulations (see legend). The dashed 1:1 line represents perfect agreement with observations. The numbers indicate the area formed by the 1:1 and model line. Numbers on the top right of each panel indicate the area between IMERG and CCAM in which the larger the number, the larger the difference between the two.

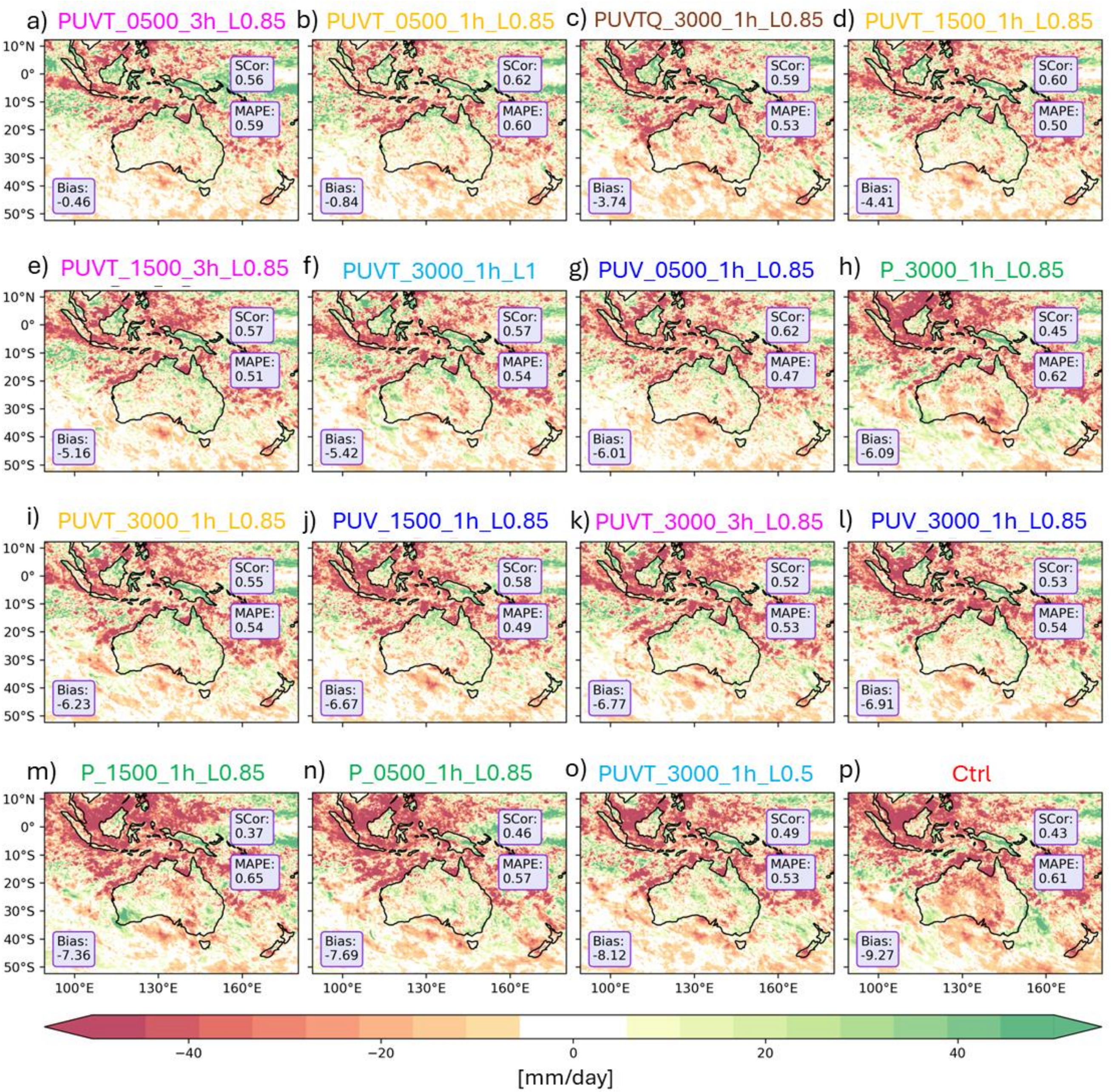

~~*Figure 10. Bias of monthly maximum 1-day precipitation (Rx1day; mm day^{-1}) from December 2010 to March 2011 relative to IMERG. Each panel shows one CCAM spectral nudging simulation (see labels), with shading indicating spatial bias across the CORDEX-Australasia domain. Statistics included in each panel are the spatial correlation (SCor), mean absolute percentage error (MAPE), and domain-averaged bias.*~~

Figure 10 illustrates the bias of monthly maximum 1-day precipitation (Rx1day) from December 2010 to March 2011, comparing 16 CCAM simulations to IMERG. Although the study period is relatively short, it is considered representative due to the extreme wet conditions associated with the 2010–2011 La Niña event. It is noteworthy that Alexander et al., (2025) used a combination of in situ, satellite, and reanalysis data to evaluate precipitation extremes (Rx1day) over land from 2001 to 2015 and found significant variability among the products in estimating regional annual wettest days. For instance, IMERG over land tends to be wetter than the Asian Precipitation -Highly Resolved Observational Data Integration Towards Evaluation of Water Resources (APHRODITE; Yatagai et al., 2012) over Monsoon Asia. Nevertheless, IMERG is used as the *"reference"* to evaluate the Rx1day from CCAM simulations in our analysis.

Figure 10 presents panels (a) to (p) arranged from the wettest to the driest simulations, where negative values (red) indicate dry biases (underestimation), and positive values (green) denote wet biases (overestimation) of extreme rainfall. The results reveal substantial variations in simulation performance. The *Ctrl* and *P_var* consistently fail to capture extreme rainfall, with Scor values $\leq$0.46, MAPEs $\geq$0.57, and significant underestimations (-7 to -9 mm day^{-1}). *PUV* and *PUVT* group at longer wavelength (e.g., 3000 km), demonstrate reasonable skill but still suffer from large dry biases (>-6 mm day^{-1}). In contrast, configurations at shorter wavelengths (e.g., *PUVT_0500_1h_L0.85* with Scor = 0.62, MAPE = 0.60, Bias = −0.84) perform better, minimizing the dry bias over the sea of MC. However, they overestimate precipitation over land regions such as Borneo, Papua New Guinea, and northern Australia.

The overestimation over northern Australia is plausible, as IMERG tends to be drier than AGCD over the Australian continent (Alexander et al., 2025, Figs. 6 and S25). In contrast, the land regions of the MC require further validation against reliable in situ observations. Overall, these rankings reinforce that short-wavelength (500 – 1500 km), low-level nudging of pressure, winds and temperature provides the most reliable representation of extremes.

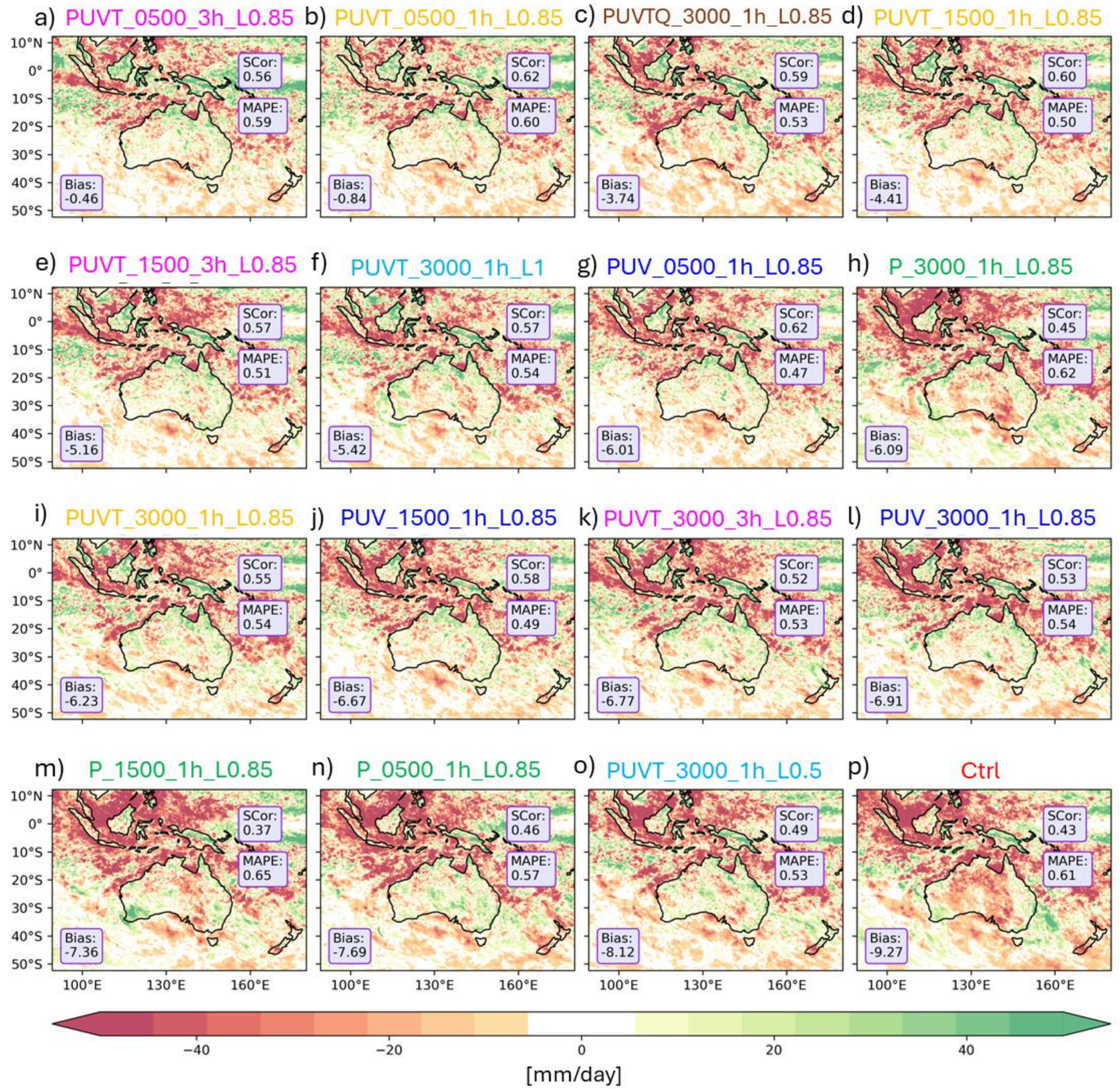

Figure 10. Bias of monthly maximum 1-day precipitation (Rx1day; mm day^{-1}) from December 2010 to March 2011 relative to IMERG. Each panel shows one CCAM spectral nudging simulation (see labels), with shading indicating spatial bias across the CORDEX–Australasia domain. Statistics included in each panel are the spatial correlation (SCor), mean absolute percentage error (MAPE), and domain-averaged bias. Panels (a)–(p) are ordered from the wettest to driest model configurations.

4 Discussion and Conclusion

This study evaluated the sensitivity of Conformal Cubic Atmospheric Model (CCAM) regional climate simulations to different spectral nudging (SN) configurations during the extreme 2010 – 11 La Niña event. Building on the work of Thatcher and McGregor (2008), who introduced the concept of scale-selective filtering for spectral nudging in CCAM, ~~The~~ the assessment aimed to examine the model's ability to reproduce large-scale circulation and regional precipitation patterns, quantify the impact of nudging settings on mean and extreme rainfall, and identify ~~optimal~~ reasonable configurations to enhance simulation during the extreme event~~fidelity~~.

Our evaluation demonstrates that spectral nudging has a decisive influence on the model's ability to reproduce both mean and extreme precipitation across Australasia. However, the effectiveness of nudging varies depending on the set of variables used, the selected wavelength, and the nudging update frequency. We found that shorter wavelength, high-frequency nudging of pressure, winds, and temperature, provides the best balance between maintaining large-scale fidelity and allowing for regional variability. This configuration consistently minimized rainfall biases (Figs. 2–4) and best captured the timing and intensity of major extreme precipitation events, such as severe tropical cyclone Cat 5 – Carlos over Darwin and Yasi over Queensland, while also reproducing the MJO phase (Fig. 5). It further reproduced realistic moisture convergence into northern Australia, ~~and~~ wind flow consistent with the monsoon and MJO-related precipitation peak locations (Fig. 6). Additionally, it aligned well with ERA5 vertical structures (Fig. 7) and produced accurate quantile distributions of extreme rainfall (Figs. 8–9). This result is consistent with previous studies (e.g., Thatcher and McGregor, 2008; Tang et al., 2017; Spero et al., 2018), which have highlighted the effectiveness of scale-selective nudging in constraining large-scale circulation while preserving mesoscale variability and extreme events.

The wavelength of the nudging plays a crucial role in determining model performance. By selecting a cut-off wavelength around 500 – 1500 km, we effectively nudged the synoptic scale of the model solution while still allowing for the development of finer-scale features. This range aligns with the findings of Gómez and Miguez-Macho (2017), who identified 1000 km as an optimal wavelength for nudging in their study. Additionally, the update frequency of 1 hour for nudging aligns with previous studies (Liu et al., 2012; Otte et al., 2012), ensuring a high degree of consistency between the nudged model and the large-scale atmospheric fields. The vertical level at which nudging is applied also influences model skill. In this study, the best performance was achieved with nudging applied above 850 hPa, consistent with findings by Wang and Kotamarthi (2013) and von Storch et al. (2000). We found that adding moisture nudging degrades the model's representation of mean and extreme precipitation, consistent with previous studies that caution against its use due to potential thermodynamic inconsistencies (Heikkila et al., 2010; Liu et al., 2012~~), although some studies have reported improvements in rainfall statistics (Omrani et al., 2015~~) and/or potential biases in ERA5 moisture fields (Virman et al., 2021; Truong et al., 2022). Configurations with longer wavelengths (e.g., 3000 km) or infrequent nudging updates (e.g., 3h) led to smoother rainfall fields, weaker extremes, and misaligned convergence zones (Fig. 3–6). This sensitivity mirrors previous studies that show overly strong or infrequent nudging degrades model performance by weakening large-scale forcing and impacting regional variability (Alexandru et al., 2009; Omrani et al., 2015). In summary, our study shows ~~demonstrates~~ that applying spectral nudging on large-scale fields above the planetary boundary layer ~~can~~ significantly improves the simulation of mean and extremes in CCAM over Australasia. The best-performing configurations, with moderate nudging wavelengths (~500–1500 km), short relaxation times (~1 h), and nudging of pressure, winds, and temperature (e.g., *PUVT_0500_1h_L0.85* and *PUVT_1500_1h_L0.85*), provide the most accurate results during the study period. However, despite improvements, the model's physical parameterisation (e.g., cloud microphysics, convection schemes) would benefit from further improvements. Further advancements in precipitation simulations and extreme events will require ongoing refinement of these parameterizations, particularly for convection schemes and cloud microphysics, especially when running higher-resolution simulations (e.g., 4 km).

~~We recommend using configurations with moderate nudging wavelengths (~500 – 1500 km), short relaxation times (~1h), and including pressure, wind, and temperature nudging for the most accurate simulations of mean and extreme rainfall. In our study, the "*PUVT_0500_1h_L0.85*" configuration achieved the highest skill across multiple diagnostics, successfully preserving large-scale circulation fidelity while allowing mesoscale processes to evolve.~~

While ~~the application of~~ spectral nudging ~~in this study has~~ significantly ~~improved~~ improves the simulation of large-scale circulation ~~and extreme precipitation events~~, the accurate representation of smaller-scale features such as extreme precipitation depends on the quality of the model's physical parameterisation ~~several limitations remain~~. Our results indicate that the best configurations for capturing extreme events may still be limited by unresolved regional processes~~Firstly, despite the improved performance of the nudged model, biases persist~~, particularly over ~~tropical convective~~the tropics, ~~and~~ mountainous regions of Papua New Guinea ~~regions~~ and coastal areas over the northern Australia such as the Gulf of Carpentaria, where the model continues to underestimate ~~s~~ extreme precipitation at the 99^{th} percentile. This limitation is likely due to ~~These persistent biases indicate that, although spectral nudging improves model accuracy,~~ missing or inadequately represented regional physical processes that influence precipitation in complex environments~~limit the simulation of extreme precipitation, especially in complex orographically influenced regions~~. It is important to note, however, that both observational and reanalysis products exhibit similar deficiencies, adding uncertainty to our model performance evaluation~~also exhibit deficiencies in these areas, which adds uncertainty to our model performance assessment~~. The ~~study's~~ 12 km ~~horizontal~~ resolution used in this study, while suitable for capturing mesoscale processes, may still miss finer-scale features like localized convection that ~~influence~~ substantially affect extreme rainfall. ~~, and h~~ Higher resolutions (e.g., 4 km) could provide a more accurate representation of these processes. Additionally, the 4-month simulation period during the 2010–11 La Niña event ~~the extreme wet summer of 2010 – 11~~ offers valuable insights, but the results are limited to this extreme event. The model's performance over different climate periods, particularly drier or less extreme seasons, may differ, suggesting that future research should include multi-year ~~could expand the time frame of~~ simulations, computational resources permitting, to assess variability and robustness across various climate conditions. The impact of GCM and reanalysis biases, which can propagate into the RCM simulation (Liu et al., 2024; Liang et al., 2008), remains another area for future research~~,~~. Integrating ~~particularly in integrating~~ bias correction techniques or multi-model ensembles

~~to enhance~~could enhance the fidelity of RCM projections. This~~Our~~ study contributes to the growing body of work on spectral nudging and its potential for enhancing regional climate simulations, particularly for applications in climate risk assessment and adaptation planning.

Author contribution

ST designed the study, carried out the analysis, and wrote the initial manuscript draft. MJT, PLN, LVA, and JLM provided supervision and contributed to manuscript review and revisions.

Competing interest

The contact author has declared that none of the authors has any competing interests.

Acknowledgement

We would also like to thank the CSIRO HPC (Petrichor) for the computational resources.

Financial support

This work is supported by the Australian Climate Service. PLN and LVA are supported by Australian Research Council (ARC) grant FT210100459. LVA is also supported by ARC grant CE230100012.

Code and data availability

The CCAM model code used in this study, including the main CCAM code (version CCAM-2504), post-processing scripts, and running scripts, is archived at Zenodo: https://doi.org/10.5281/zenodo.19018138. The observational and reanalysis datasets used in this study (ERA5, GPCP, CMORPH, and IMERG precipitation data) is archived at Zenodo: https://doi.org/10.5281/zenodo.19077484. Original datasets remain available from their providers:

- ERA5 (Hersbach et al., 2023): https://doi.org/10.24381/cds.bd0915c6
- GPCP (Huffman et al., 2023): https://doi.org/10.5067/MEASURES/GPCP/DATA305
- CMORPH (Joyce et al., 2004; Xie et al., 2017): https://doi.org/10.25921/w9va-q159
- IMERG (Huffman et al., 2019): https://doi.org/10.5067/GPM/IMERGDF/DAY/06

All figures presented in this manuscript were generated using Python scripts, which are publicly available at https://doi.org/10.5281/zenodo.18423588. All references of the datasets are listed in the in-text data citation references.

Reference

Alexandru, A., de Elía, R., Laprise, R., Separovic, L., ~~&~~ Biner, S. (2009). Sensitivity study of regional climate model simulations to large-scale nudging parameters. Monthly Weather Review, 137(5), 1666–1686. https://doi.org/10.1175/2008MWR2620.1

Alexander, L. V., and Coauthors, 2025: Less intense daily precipitation maxima in regional compared to global gridded products. J. Climate, https://doi.org/10.1175/JCLI-D-25-0222.1, in press.

Alexander, L. V., Bador, M., Roca, R., Contractor, S., Donat, M. G., and Nguyen, P. L. (2020)~~:~~ Intercomparison of annual precipitation indices and extremes over global land areas from in situ, space-based and reanalysis products, Environ. Res. Lett., 15, 055002, https://doi.org/10.1088/1748-9326/ab79e2~~, 2020~~.

BoM (2012). Record-breaking La Niña events: An analysis of the La Niña life cycle and the impacts and significance of the 2010–11 and 2011–12 La Niña events in Australia. Bureau of Meteorology, Commonwealth of Australia.

Cai, W., ~~&~~ van Rensch, P. (2012). The 2011 southeast Queensland extreme summer rainfall: A confirmation of a shift in the interdecadal Pacific oscillation? Geophysical Research Letters, 39(8), L08702. https://doi.org/10.1029/2011GL050820

~~Castro, C. L., Pielke Sr, R. A., & Leoncini, G. (2005). Dynamical downscaling: Assessment of value retained and added using the Regional Atmospheric Modeling System (RAMS). Journal of Geophysical Research, 110(D5), D05108. https://doi.org/10.1029/2004JD004721~~

Cha, D. H., Jin, C. S., Lee, D. K., ~~&~~ Kuo, Y. H. (2011). Impact of intermittent spectral nudging on regional climate simulation using WRF. Journal of Geophysical Research: Atmospheres, 116(D10), D10103. https://doi.org/10.1029/2010JD015069

Chapman, S., Syktus, J., Trancoso, R., Toombs, N. ~~&~~ Eccles, R (2024)~~.~~ Projected changes in mean climate and extremes from downscaled high-resolution CMIP6 simulations in Australia. Weather and Climate Extremes 46, 100733, https://doi.org/10.1016/j.wace.2024.100733 ~~(2024)~~.

Chapman, S., Syktus, J., Trancoso, R., Thatcher, M., Toombs, N., Wong, K. K-H., Takbash, A. (2023). Evaluation of dynamically downscaled CMIP6-CCAM models over Australia. Earth's Future, 11, e2023EF003548. https://doi.org/10.1029/2023EF003548

Choi SJ, Lee DK. 2015. Impact of spectral nudging on the downscaling of tropical cyclones in regional climate simulations. Adv. Atmos. Sci. 33: 730–742.

Evans, J. P., Boyer-Souchet, I., ~~&~~ Olson, R. (2012). Local sea surface temperatures add to extreme precipitation in northeast Australia during La Niña. Geophysical Research Letters, 39(10), L10803. https://doi.org/10.1029/2012GL052014

Evans, J. P., Marchand, R., ~~&~~ Ackerman, T. (2014). Variability of Australian monsoon precipitation in the last 60 years. Journal of Climate, 27(15), 5859–5870. https://doi.org/10.1175/JCLI-D-13-00422.1

Feser, F. (2012). Regional climate models add value to global model data: A review and selected examples. Environmental Research Letters, 7(1), 014024. https://doi.org/10.1088/1748-9326/7/1/014024

Feser, F., and M. Barcikowska (2012), The influence of spectral nudging on typhoon formation in regional climate models, Environ. Res. Lett., 7(1), 14,024.

Freidenreich, S. M., and V. Ramaswamy. 1999. “A New Multiple-Band Solar Radiative Parameterization for General Circulation Models.” Journal of Geophysical Research: Atmospheres 104: 31389–31409.

Giorgi, F. (2019). Thirty years of regional climate modeling: Where are we and where are we going next? Journal of Geophysical Research: Atmospheres, 124(11), 5696–5723. https://doi.org/10.1029/2018JD030094

Giorgi, F., & Mearns, L. O. (1999). Introduction to special section: Regional climate modeling revisited. Journal of Geophysical Research: Atmospheres, 104(D6), 6335–6352. https://doi.org/10.1029/98JD02072

Gibson, P. B., Lewis, H., Campbell, I., Rampal, N., Fauchereau, N.,~~ &~~ Harrington, L. J. (2025). Downscaled climate projections of tropical and ex-tropical cyclones over the southwest Pacific. Journal of Geophysical Research: Atmospheres, 130, e2025JD043833. https://doi.org/10.1029/2025JD043833

Gibson, P.B., Stuart, S., Sood, A. et al. Dynamical downscaling CMIP6 models over New Zealand: added value of climatology and extremes. Clim Dyn 62, 8255–8281 (2024). https://doi.org/10.1007/s00382-024-07337-5

Giles, B.D. (2012), The Australian Summer 2010/2011. Weather, 67: 9-12. https://doi.org/10.1002/wea.860

Gómez, B. and Miguez-Macho, G. (2017), The impact of wave number selection and spin-up time in spectral nudging. Q.J.R. Meteorol. Soc, 143: 1772-1786. https://doi.org/10.1002/qj.3032

Grose, M. R., Narsey, S., Delage, F., Dowdy, A. J., Bador, M., Boschat, G., et al. (2020). Insights from CMIP6 for Australia’s future climate. Earth’s Future, 8(5), e2019EF001469. https://doi.org/10.1029/2019EF001469

Huang, Z., Zhong, L., Ma, Y., and Fu, Y. (2021) Development and evaluation of spectral nudging strategy for the simulation of summer precipitation over the Tibetan Plateau using WRF (v4.0), Geosci. Model Dev., 14, 2827–2841, https://doi.org/10.5194/gmd-14-2827-2021

Heikkila, U., Sandvik, A., and Sorteberg, A. (2010)~~:~~ Dynamical downscaling of ERA-40 in complex terrain using the WRF regional climate model, Clim. Dynam., 37, 1551–1564, https://doi.org/10.1007/s00382-010-0928-6~~, 2010~~.

Hersbach, H., Bell, B., Berrisford, P., Hirahara, S., Horányi, A., Muñoz-Sabater, J., Nicolas, J., Peubey, C., Radu, R., Schepers, D., Simmons, A., Soci, C., Abdalla, S., Abellan, X., Balsamo, G., Bechtold, P., Biavati, G., Bidlot, J., Bonavita, M., De Chiara, G., Dahlgren, P., Dee, D., Diamantakis, M., Dragani, R., Flemming, J., Forbes, R., Fuentes, M., Geer, A., Haimberger, L., Healy, S., Hogan, R. J., Hólm, E., Janisková, M., Keeley, S., Laloyaux, P., Lopez, P., Lupu, C., Radnoti, G., de Rosnay, P., Rozum, I., Vamborg, F., Villaume, S., and Thépaut, J.-N~~.:~~. (2020) The ERA5 global reanalysis, Q. J.Roy. Meteor. Soc., 146, 1999–2049, https://doi.org/10.1002/qj.3803~~, 2020~~.

Hersbach, H., Bell, B., Berrisford, P., Biavati, G., Horányi, A., Muñoz Sabater, J., Nicolas, J., Peubey, C., Radu, R., Rozum, I., Schepers, D., Simmons, A., Soci, C., Dee, D., and Thépaut, J.-N~~.:~~. (2023) ERA5 hourly data on pressure levels from 1940 to present, Copernicus Climate Change Service (C3S) Climate Data Store (CDS) [data set], https://doi.org/10.24381/cds.bd0915c6~~, 2023~~.

Hoffmann, P., Katzfey, J.J., McGregor, J.L., Thatcher, M., (2016). Bias and variance correction of sea surface temperatures used for dynamical downscaling. J. Geophys. Res. Atmos. 121 (21), 12877–812890. https://doi.org/10.1002/2016JD025383.

Howard, E., Su, C.-H., Stassen, C., Naha, R., Ye, H., Pepler, A., Bell, S. S., Dowdy, A. J., Tucker, S. O., and Franklin, C.: Performance and process-based evaluation of the BARPA-R Australasian regional climate model version 1, Geosci. Model Dev., 17, 731–757, https://doi.org/10.5194/gmd-17-731-2024, 2024.

Huffman, G. J., Stocker, E. F., Bolvin, D. T., Nelkin, E. J.,~~ &~~ Tan, J. (2019). GPM IMERG final precipitation L3 1 day 0.1 degree x 0.1 degree V06. In A. Savtchenko & M. D. Greenbelt (Eds.), Goddard earth sciences data and information services center (GES DISC). https://doi. org/10.5067/GPM/IMERGDF/DAY/06

Huffman, G. J., R. F. Adler, A. Behrangi, D. T. Bolvin, E. J. Nelkin, G. Gu, and M. R. Ehsani, 2023: The New Version 3.2 Global Precipitation Climatology Project (GPCP) Monthly and Daily Precipitation Products. J. Climate, 36, 7635–7655, https://doi.org/10.1175/JCLI-D-23-0123.1.

Hurley, P. 2007. "Modelling Mean and Turbulence Fields in the Dry Convective Boundary Layer With the Eddy-Diffusivity/Mass-Flux Approach." Boundary-Layer Meteorology 125: 525–536. https://doi.org/ 10.1007/s10546-007-9203-8.

Hong, S. Y., ~~&~~ Chang, E. C. (2012). Spectral nudging sensitivity simulations in a regional climate model. Asia-Pacific Journal of Atmospheric Sciences, 48(4), 345–355. https://doi.org/10.1007/s13143-012-0033-3

Imran, H.M., Evans, J.P. Observational uncertainty in the added value of regional climate modelling over Australia. Clim Dyn 63, 73 (2025). https://doi.org/10.1007/s00382-024-07562-y

Isphording, R. N., Alexander, L. V., Bador, M., Green, D., Evans, J. P., and Wales, S. (2024)~~:~~ A Standardized Benchmarking Framework to Assess Downscaled Precipitation Simulations, J. Climate, 37, 1089–1110, https://doi.org/10.1175/JCLI-D-23-0317.1~~, 2024~~.

IPCC, 2021: Climate Change (2021)~~:~~ The Physical Science Basis. Contribution of Working Group I to the Sixth Assessment Report of the Intergovernmental Panel on Climate Change. Cambridge University Press, Cambridge, United Kingdom and New York, NY, USA, In press, doi:10.1017/9781009157896.

Jin, C. S., Cha, D. H., Lee, D. K., Suh, M. S., Hong, S. Y., Kang, H. S.,~~ &~~ Ho, C. H. (2016). Evaluation of climatological tropical cyclone activity over the western North Pacific in the CORDEX-East Asia multi-RCM simulations. Climate Dynamics, 47(3), 765–778. https://doi.org/10.1007/s00382-015-2869-6

Joyce, R. J., J. E. Janowiak, P. A. Arkin, and P. Xie, (2004)~~:~~ CMORPH: A Method that Produces Global Precipitation Estimates from Passive Microwave and Infrared Data at High Spatial and Temporal Resolution. Journal of Hydrometeorology, 5, 487-503 (DOI: 10.1175/1525-7541(2004)005<0487:CAMTPG>2.0.CO;2).

Jones, D. A., W. Wang, and R. Fawcett, 2009: High-quality spatial climate data-sets for Australia. Aust. Meteor. Oceanogr. J., 58, 233–248, https://doi.org/10.22499/2.5804.003.

Karoly, D.J. and Boulter, S. (2013) Afterword: floods, storms, fires and pestilence – disaster risk in Australia during 2010–2011. In: S. Boulter, J. Palutikof, D.J. Karoly and D. Guitart (eds) Natural Disasters and Adaptation to Climate Change. Cambridge University Press, Cambridge, pp. 252–261.

Kanamitsu, M., & Kanamaru, H. (2007). Fifty-seven-Year California reanalysis downscaling at 10 km (CaRD10). Part I: System detail and validation with observations. Journal of Climate, 20(22), 5553–5571. https://doi.org/10.1175/2007JCLI1482.1

Lai, W., & Gan, J. (2025). On spectral nudging and dynamics to improve representation of marine cloud and precipitation over the China sea in summer. Theoretical and Applied Climatology, 156(8), 444.

Liang, X.-Z., K. E. Kunkel, G. A. Meehl, R. G. Jones, and J. X. L. Wang (2008), Regional climate models downscaling analysis of general circulation models present climate biases propagation into future change projections, Geophys. Res. Lett., 35, L08709, doi:10.1029/2007GL032849.

Liu, S., Zeman, C.,~~ &~~ Schär, C. (2024). Dynamical downscaling of climate simulations in the tropics. GeophysicalResearch Letters, 51, e2023GL105733.https://doi.org/10.1029/2023GL105733

Liu, Y. L., Alexander, L. V., Evans, J. P.,~~&~~ Thatcher, M. (2024). Sensitivity of Australian rainfall to driving SST datasets in a variable-resolution global atmospheric model. Journal of Geophysical Research: Atmospheres, 129, e2024JD040954 https://doi.org/10.1029/2024JD040954

Liu P, Tsimpidi AP, Hu Y, Stone B, Russell AG, Nenes A. 2012. Differences between downscaling with spectral and grid nudging using WRF. Atmos. Chem. Phys. 12: 3601–3610. https://doi.org/10.5194/acp-12-3601-2012.

Lisonbee, J. and Ribbe, J~~.: ~~. (2021) Seasonal climate influences on the timing of the Australian monsoon onset, Weather Clim. Dynam., 2, 489–506, https://doi.org/10.5194/wcd-2-489-2021~~, 2021~~.

Ma, S., Trancoso, R., Syktus, J., Chapman, S.,~~ &~~ Eccles, R. (2025). Evaluating ERA5 downscaled simulations using CCAM: Large-scale circulation processes and teleconnections. Journal of Geophysical Research: Atmospheres, 130, e2025JD043566. https://doi.org/10.1029/2025JD043566

Mai X, Qiu X, Yang Y, Ma Y (2020) Impacts of spectral nudging parameters on dynamical downscaling in summer over Mainland China. Front Earth Sci 8.

McGregor, J. L. (2003)~~.~~ "A New Convection Scheme Using a Simple Closure." BMRC Research Report 93: 33–36.

McGregor, J. L., and M. R. Dix. (2008)~~.~~ "An Updated Description of the Conformal-Cubic Atmospheric Model." In High Resolution Numerical Modelling of the Atmosphere and Ocean, edited by K. Hamilton and W. Ohfuchi. Springer. https://doi.org/10.1007/978-0-387-49791-4_4.

Miguez-Macho, G., G. L. Stenchikov, and A. Robock, (2004)~~:~~ Spectral nudging to eliminate the effects of domain position and geometry in regional climate model simulations. J. Geophys. Res., 109, D13104, https://doi.org/10.1029/2003JD004495.

Menut, L., Bessagnet, B., Cholakian, A., Siour, G., Mailler, S., and Pennel, R. (2024)~~:~~ What is the relative impact of nudging and online coupling on meteorological variables, pollutant concentrations and aerosol optical properties?, Geosci. Model Dev., 17, 3645–3665, https://doi.org/10.5194/gmd-17-3645-2024~~, 2024.~~

Narsey S et al. (2025) Disentangling the uncertainties in regional projections for Australia. Journal of Southern Hemisphere Earth Systems Science 75, ES25015. doi:10.1071/ES25015

Nguyen, P. L., Alexander, L. V., Thatcher, M. J., Truong, S. C. H., Isphording, R. N., and McGregor, J. L. (2024)~~:~~ Selecting CMIP6 global climate models (GCMs) for Coordinated Regional Climate Downscaling Experiment (CORDEX) dynamical downscaling over Southeast Asia using a standardised benchmarking framework, Geosci. Model Dev., 17, 7285–7315, https://doi.org/10.5194/gmd-17-7285-2024~~, 2024.~~

Nguyen, P.-L., Bador, M., Alexander, L. V., Lane, T. P., and Ngo-Duc, T. (2022)~~:~~ More intense daily precipitation in CORDEX-SEA regional climate models than their forcing global climate models over Southeast Asia, Int. J. Climatol., 42, 6537–6561, https://doi.org/10.1002/joc.7619~~, 2022~~

Nguyen, P.-L., Bador, M., Alexander, L. V., Lane, T. P., and Funk, C. C. (2020)~~:~~ On the Robustness of Annual Daily Precipitation Maxima Estimates Over Monsoon Asia, Frontiers in Climate, 2, 578785, https://doi.org/10.3389/fclim.2020.578785~~, 2020~~

Otte, T. L., Nolte, C. G., Otte, M. J., and Bowden, J. H.: Does Nudging Squelch the Extremes in Regional Climate Modeling?, J. Climate, 25, 7046–7066, https://doi.org/10.1175/JCLI-D-12-00048.1, 2012.

Omrani, H., Drobinski, P., Dubos, T.,~~ &~~ Turuncoglu, U.~~ U.~~ (2015). Optimal nudging strategies in regional climate modeling: Investigation in a Big-Brother simulation over the Euro-Mediterranean region. Climate Dynamics, 44(5–6), 1559–1577. https://doi.org/10.1007/s00382-014-2453-5

Rotstayn, L. D., and U. Lohmann (~~.~~2002). “Simulation of the Tropospheric Sulfur Cycle in a Global Model With a Physically Based Cloud Scheme.” Journal of Geophysical Research: Atmospheres 107, no. D21: AAC 20-1–AAC 20-21. https://doi.org/10.1029/2002JD002128.

Schroeter, B. J. E., B. Ng, A. Takbash, T. Rafter, and M. Thatcher, (2024): A Comprehensive Evaluation of Mean and Extreme Climate for the Conformal Cubic Atmospheric Model (CCAM). J. Appl. Meteor. Climatol., 63, 997–1018, https://doi.org/10.1175/JAMC-D-24-0004.1.

Schwarzkopf, M. D., and V. Ramaswamy ~~.~~(1999). “Radiative Effects of CH4, N2O, Halocarbons and the Foreign-Broadened H2Ocon-Tinuum: A GCM Experiment.” Journal of Geophysical Research: Atmospheres 104: 9467–9488.

Spero, T. L., Nolte, C. G., Bowden, J. H.,~~ &~~ Mallard, M. S. (2018). Sensitivity of WRF simulations to different spectral nudging techniques. Journal of Applied Meteorology and Climatology, 57(6), 1303–1320. https://doi.org/10.1175/JAMC-D-17-0098.1

Su C, Torrance J, Rennie S, Howard E, Stassen C, Warren R, Smith A, Dharssi I, Pepler A, Tian S, Lipson M, Steinle P, Franklin C, Le T, Wang C, Masoumi S, Le Marshall J. (2025) The Australian regional atmospheric reanalysis system, version 2 – BARRA2. Journal of Southern Hemisphere Earth Systems Science 75, ES25032. https://doi.org/10.1071/ES25032

Spero, T. L., Otte, M. J., Bowden, J. H., and Nolte, C. G.: Improving the representation of clouds, radiation, and precipitation using spectral nudging in the Weather Research and Forecasting model, J. Geophys. Res.-Atmos., 119, 11682–11694, https://doi.org/10.1002/2014JD022173, 2014.

~~Tang, J., Song, S., & Wu, J. (2009). Impacts of the spectral nudging technique on simulation of the East Asian summer monsoon. Theoretical and Applied Climatology, 101(1–2), 41–51. https://doi.org/10.1007/s00704-009-0202-1~~

Tang, J., Wang, S., Niu, X., Hui, P., Zong, P., ~~&~~ Wang, X. (2017). Impact of spectral nudging on regional climate simulation over CORDEX East Asia using WRF. Climate Dynamics, 48(7–8), 2339–2357. https://doi.org/10.1007/s00382-016-3208-2

Thatcher, M., & McGregor, J. L. (2008). Using a scale-selective filter for dynamical downscaling with the conformal cubic atmospheric model. Monthly Weather Review, 136(2), 4578–4596. https://doi.org/10.1175/2008MWR2599.1

Thatcher, M., and P. Hurley. (2012). “Simulating Australian Urban Climate in a Mesoscale Atmospheric Numerical Model.” Boundary Layer Meteorology 142: 149–175.

Truong, S. C. H., Ramsay, H. A., Rafter, T., ~~&~~ Thatcher, M. J. (2025). Simulation of an intense tropical cyclone in the conformal cubic atmo-spheric model and its sensitivity to horizontal resolution. Weather and Climate Extremes, 47, 100744. https://doi.org/10.1016/j.wace.2025.100744

Truong, S. C. H., ~~&~~ Thatcher, M. (2025). Evaluation of clouds in the conformal cubic atmospheric model using the CFMIP observation simulator package. International Journal of Climatology, 45(8), e8846. https://doi.org/10.1002/joc.8846

Truong, S.C.H.*, Y. Huang, S. T. Siems, M. J. Manton, and F. Lang, Biases in the thermodynamic structure over the Southern Ocean in ERA5 and their radiative implications. International Journal of Climatology. https://doi.org/10.1002/joc.7672

Ummenhofer, C. C., Sen Gupta, A., Briggs, P. R., England, M. H., McIntosh, P. C., Meyers, G. A., et al. (2015). How did ocean warming affect Australian rainfall extremes during the 2010–2011 La Niña event? Geophysical Research Letters, 42(3), 9942–9951. https://doi.org/10.1002/2015GL065947

Virman, M., Bister, M., Räisänen, J., Sinclair, V. A., & Järvinen, H. (2021). Radiosonde comparison of ERA5 and ERA-Interim reanalysis datasets over tropical oceans. Tellus A: Dynamic Meteorology and Oceanography, 73(1), 1–7. https://doi.org/10.1080/16000870.2021.1929752

von Storch, H., Langenberg, H., ~~&~~ Feser, F. (2000). A spectral nudging technique for dynamical downscaling purposes. Monthly Weather Review, 128(10), 3664–3673. https://doi.org/10.1175/1520-0493(2000)128<3664:ASNTFD>2.0.CO;2

Wang J, Kotamarthi VR. (2013). Assessment of dynamical downscaling in near-surface fi elds with different spectral nudging approaches using the nested regional climate model (NRCM). J. Appl. Meteorol. Climatol. 52: 1576–1591. https://doi.org/10.1175/JAMC-D-12-0302.1.

Xie, P., R. Joyce, S. Wu, S. Yoo, Y. Yarosh, F. Sun, and R. Lin, (2017): Reprocessed, Bias-Corrected CMORPH Global High-Resolution Precipitation Estimates from 1998. J. Hydrometeor., 18, 1617-1641 (DOI: 10.1175/JHM-D-16-0168.1).

Yatagai, A., K. Kamiguchi, O. Arakawa, A. Hamada, N. Yasutomi, and A. Kitoh, (2012): APHRODITE: Constructing a Long-Term Daily Gridded Precipitation Dataset for Asia Based on a Dense Network of Rain Gauges. Bull. Amer. Meteor. Soc., 93, 1401–1415, https://doi.org/10.1175/BAMS-D-11-00122.1.

Zhang, H., Chapman, S., Trancoso, R., Toombs, N., & Syktus, J. (2024). Assessing the impact of bias correction approaches on climate extremes and the climate change signal. Meteorological Applications, 31(3), e2204. https://doi.org/10.1002/met.2204

~~Yhang, Y. B., & Hong, S. Y. (2011). A study on large-scale nudging effects in regional climate model simulation. Asia-Pacific Journal of Atmospheric Sciences, 47(3), 235–243. https://doi.org/10.1007/s13143-011-0012-0~~